Alzheimer's disease (AD) is the most prevalent cause of dementia and is characterized by loss of memory and cognition as well as behavioral and occupational instability in old age. One of the pathological characteristics of AD is the progressive deposition of insoluble amyloid β protein (Aβ) as a form of senile plaques (Wirths *et al.* 2004). This protein comprises peptides of approximately 39 to 43 amino acid residues derived from the transmembrane amyloid precursor protein (APP) (Selkoe 2002). Aβ can form monomers and a variety of different aggregate morphologies including dimers, small soluble oligomers, protofibrils, diffuse plaques, and fibrillar deposits seen in the senile plaques. Protofibrils, diffuse plaques, and fibrillar deposits seem to have a predominant β-sheet structure (Tierney *et al.* 1988; Barrow and Zagorski 1991), while oligomers are believed to be more globular (Barghorn *et al.* 2005). Increasing evidence that the formation of these aggregates, particularly oligomer, causes primary neurodegeneration in AD has led to the amyloid hypothesis which states that the accumulation of Aβ in the CNS is highly neurotoxic and deteriorates synaptic functions (Selkoe 2002; Wirths *et al.* 2004). Moreover, several lines of evidence suggest that Aβ accumulation begins at relatively early stages before cognitive decline becomes manifest (Anderton *et al.* 1998; Selkoe 2002). Therefore, it is hypothesized that the formation, deposition, and aggregation of Aβ in the brain should be primary targets for complete amelioration of dementia. Currently, drugs available for dementia such as acetylcholinesterase inhibitors exert only a temporary benefit on cognitive dysfunction (Millard and Broomfield 1995; Park *et al.* 2000; Darreh-Shori *et al.* 2004), and they do not prevent or reverse the formation of Aβ deposits. One potentially promising strategy for developing more effective anti-dementia drugs is the inhibition of Aβ fibril formation or destabilization of aggregated Aβ or a combination of both.

Herbal remedies are used worldwide and have a long history of use in alleviating a variety of symptoms of many different conditions and diseases. Recently, clinical trials in AD patients have also shown that some of these traditional medications improved Mini-Mental State Examination scores, P300 latency, and blood flow in the cerebral cortex (Le Bars *et al.* 1997). Although inconclusive, these provocative studies suggest that even old remedies can be beneficial in AD and related disorders. We have reported that several traditional herbal medicines such as *Formula lienalis angelicae compositae* (kamiuntanto) (Suzuki *et al.* 2001; Nakagawasai *et al.* 2004), *Pilulae octo-medicamentorum rehmanniae* (hachimijiogan) (Iwasaki *et al.* 2004), and *Pulvis depressionis hepatis* (yokukansan) (Iwasaki *et al.* 2005) improved symptoms of dementia. The radicis cortex of *Paeonia suffruticosa* (*Moutan cortex*; Botan-pi), a major medicinal plant comprising *Pilulae octo-medicamentorum rehmanniae*, is used as an anti-pyretic and anti-inflammatory agent (Lin *et al.* 1999; Yasuda *et al.* 1999; Chou 2003). Paeonol, a common component of *Paeonia suffruticosa*, has been shown to inhibit platelet aggregation in rabbits (Lin *et al.* 1999) as well as to reduce cerebral infarction in ischemia-reperfusion-injured rats (Hsieh *et al.* 2006). However, the underlying mechanism of traditional medicinal herbs, including *Paeonia suffruticosa*, on the formation and metabolism of Aβ fibrils has never been investigated. In the present study, we examined the effect of *Paeonia suffruticosa* on the formation of Aβ aggregates and its ability to destabilize pre-formed Aβ fibrils *in vitro* by using fluorescence spectroscopy with thioflavin T.

1,2,3,4,6-Penta-*O*-galloyl-β-D-glucopyranose (PGG), a high molecular weight tannin-type polyphenols, has been isolated from *Paeonia suffruticosa*. The defining characteristic of tannins is their ability to bind and precipitate proteins (Hofmann *et al.* 2006). Li *et al.* (2005) previously reported that PGG could bind to insulin receptors and activate an insulin-mediated glucose transport signaling pathway. However, the effect of this compound on the formation and metabolism of Aβ fibrils has not yet been investigated.

Our results provide strong evidence that several traditional herbs extracts including *Paeonia suffruticosa* and PGG have inhibitory and destabilizing effects on Aβ fibrils.

Materials and methods

Reagents

Aβ peptides (1–40 and 1–42) and thioflavin-T were obtained from Peptide Institute (Osaka, Japan) and from Sigma (St Louis, MO, USA), respectively. All the reagents and drugs used were of analytical grade.

Preparation of medicinal herb extracts

Water, 100% methanol, and 99.5% ethanol extracts of medicinal herbs were prepared by refluxing 10 g of sliced dry herbs in 100 mL of each solution for 30 min. The decoction after cooling to 25°C was evaporated completely under reduced pressure to yield dried or oily extracts. The extracts were weighed and dissolved in dimethylsulfoxide at a concentration of 100 mg/mL and then stored at −20°C. When assaying, these extracts were dissolved in 50 mM potassium phosphate buffer (pH 7.4) and the solutions were adjusted to pH 7.4 when necessary.

Analysis of three-dimensional HPLC fingerprints of water extract of *Paeonia suffruticosa*

Paeonia suffruticosa (0.5 g) was extracted with 30 mL of distilled water under ultrasonication for 30 min. The solution was filtered and then analyzed by HPLC. The HPLC system consisted of an HPLC pump (LC-10AD; Shimadzu, Kyoto, Japan) and a TSK-GEL 80_{TS} column (4.6 mm × 250 mm), and (A) 50 mM acetic acid-ammonium acetate and (B) acetonitrile were used as the eluents. A linear gradient of 90% A and 10% B changing over 60 min to 0% A and 100% B was used. The flow rate was controlled at 1.0 mL/min. After the eluate was obtained from the column, the three-dimensional data were processed with a diode array detector (SPD-M10A; Shimadzu).

Thioflavin-T measurement

Thioflavin-T measurement was performed using the method described by Suemoto *et al.* (2004) with slight modifications. For the Aβ aggregate-formation assay, Aβ (20 μM) dissolved in the 50 mM potassium phosphate buffer (pH 7.4) with a test herbal extract was incubated at 37°C for 96 h ($A\beta_{1-40}$) or 24 h ($A\beta_{1-42}$). For the destabilization assay of pre-formed Aβ aggregates, after incubation of $A\beta_{1-40}$ (96 h) or $A\beta_{1-42}$ (24 h) without a test herbal extract, a mixture of the aggregated Aβ and a test herbal extract was incubated for 30 min at 37°C.

At the end of the incubation, 3 μM thioflavin-T dissolved in 100 mM glycine buffer (pH 8.5) was added to the mixture. Fluorescence of thioflavin-T bound to Aβ aggregates was measured using a microplate reader (Spectramax GEMINI XS; Molecular Devices, Sunnyvale, CA, USA) (excitation at 442 nm and emission at 485 nm) after incubation for 30 min at 25°C. The percentage inhibition was calculated by comparing the fluorescence values of test samples with those of control solutions without herbal extracts.

Animals

Tg2576 APPswe mice over-express a 695-amino acid splice form (Swedish mutation K670N M671I) of the human Aβ precursor protein (APP695) which resulted in a fivefold increase in $A\beta_{1-40}$ and a 14-fold increase in $A\beta_{1-42}$ with increasing age, driven by the hamster prion protein promoter. The animals were allowed free access to water and standard laboratory food in a facility with the temperature controlled at 24 ± 1°C and relative humidity at 55 ± 5%, with lights on from 7:00 to 19:00 hours daily. Behavioral studies were performed between 10:00 and 12:00 hours. Experimental protocols were approved by the Animal Care and Use Committee, Tohoku University Graduate School of Medicine, and complied with the procedures outlined in the Guide for the Care and Use of Laboratory Animals of Tohoku University.

Step-through passive-avoidance test

The apparatus (AP model; O'Hara Co., Tokyo, Japan) for the step-through passive-avoidance test consisted of two compartments, illuminated compartment [100 mm × 120 mm × 100 mm; light at the top of compartment (27W, 3000 lx)] and dark compartment (100 mm × 170 mm × 100 mm). The compartments were separated by a guillotine door. During the learning stage, a mouse was placed in the illuminated safe compartment. As the compartment was lit, the mouse stepped through the opened guillotine door into the dark compartment. The time spent in the illuminated compartment was defined as the latency time. Three seconds after the mouse entered the dark compartment, a foot shock (0.3 mA, 50V, 50 Hz ac, for 3 s) was delivered to the floor grids in the dark compartment. The mouse could escape from the shock only by stepping back to the safe illuminated compartment. Such acquisition trials during the learning stage were carried out once a day for 5 days. It was judged as learning avoidance from foot-shock if the mouse remained in the illuminated compartment for 300 s after being placed there. The retention trials were carried out once per week for 10 weeks from Days 8 to 78 to evaluate the retention of avoidance memory. The latency time was measured for up to 300 s without delivering foot-shock. It was judged that the mouse retained the avoidance memory when it stayed in the illuminated safe compartment for 300 s. Acquisition and retention trials were conducted in 11-month-old mice.

Immunocytochemistry

All sample brains were fixed in neutral-buffered formalin and embedded in paraffin. Immunocytochemistry was performed using an Amyloid β Protein Immunohistostain Kit (Wako Pure Chemical Industries, Ltd., Osaka, Japan) according to the manufacturer's instructions. Briefly, after deparaffinization, 8-μm brain sections were immersed in 99% formic acid for 5 min, blocked with blocking serum, and immunostained with BA27 ($A\beta_{1-40}$) and BC05 ($A\beta_{1-42}$) by a standard avidin–biotin complex method, using 3,3′-diaminobenzidine as chromogen and lightly counter-staining with hematoxylin.

Tissue preparation

Tissue samples were processed in Tris-buffered saline (soluble fraction) and 70% formic acid (insoluble fraction) containing 1× protease inhibitor mixtures as described previously (Calon *et al.* 2004) with slight modifications. Briefly, brain tissues were homogenized and sonicated in Tris-buffered saline containing protease inhibitor mixture. The resulting homogenate was subjected to ultracentrifugation at 200 000 *g* at 4°C for 20 min, and the soluble supernatant was collected and frozen. To analyze the insoluble Aβ, the insoluble pellet was sonicated in 200 μL of 70% formic acid and subjected to ultracentrifugation at 300 000 *g* at 4°C for 30 min, and the soluble supernatant was collected.

Aβ levels

Brain $A\beta_{1-40}$ and $A\beta_{1-42}$ levels were measured using sandwich ELISA with a Human β Amyloid ELISA Kit (Wako Pure Chemical Industries, Ltd.) according to the manufacturer's instructions. BAN50 is a monoclonal antibody raised against a synthetic peptide of human $A\beta_{1-16}$; it preferentially reacts with the N-terminal portion of human Aβ starting at Asp-1 but does not cross-react with N-terminally truncated Aβ nor with rodent-type Aβ. BA27 and BC05, which specifically recognize the C terminus of $A\beta_{1-40}$ and $A\beta_{1-42}$, respectively, were conjugated with horseradish peroxidase and used as detector antibodies. Mice brain insoluble fractions described above were neutralized and subjected to BAN50/BA27 or BAN50/BC05 ELISA. The amount of Aβ was calculated by comparing these absorbance values with those of control solutions without herbal extract.

Aβ oligomerization analysis

Amount of $A\beta_{1-42}$ oligomer was measured using Aβ Aggregate Human Singleplex Bead Kit (Invitrogen Corporation, Carlsbad, CA, USA) according to the manufacturer's instructions. Data analysis was performed by a flow cytometer (FACSCaliber, Becton Dickinson Immunocytometry Systems, Franklin Lakes, NJ, USA).

Cell viability assay

SK-N-SH cells were maintained in Dulbecco's modified Eagle's medium (Gibco Life Technologies, Carlsbad, CA, USA) supplemented with 10% fetal calf serum and 4 mM L-glutamine in a humidified atmosphere of 5% CO_2 and 95% air. SK-N-SH cells were seeded in 96-well plates at a density of 1×10^4 cells per well. After 24 h, we pre-incubated SK-N-SH cells for 30 min with PGG, followed by 24 h treatment with 10 μM aggregated $A\beta_{1-42}$. Cell

viability was assessed using the 3-(4,5-dimethylthiazol-2-yl)-2,5-diphenyltetrazolium bromide (MTT) method. Absorbance values of formazan were determined at 590 nm with an automatic microplate reader.

Data analysis

Data were expressed as mean ± SD. Statistical comparisons were made using ANOVA with Bonferroni's *post hoc* analysis. $p < 0.05$ was considered to be significant.

Results

Concentration-dependent effects of *Paeonia suffruticosa* on kinetics of Aβ fibril formation and breakdown

In our previous publication, it was noted that several medicinal herbs including *Uncaria rhynchophylla*, *Cinnamomum cassia*, and *Paeonia suffruticosa* showed destabilizing activity on Aβ fibrils (Fujiwara *et al.* 2006). *Paeonia suffruticosa* which was extracted either by water, methanol, or ethanol was concentrated under reduced pressure to yield oily residues (2.33, 1.89, and 2.14 g for water, methanol, and ethanol, respectively). To examine the inhibitory effect of *Paeonia suffruticosa* on Aβ fibril formation, concentration-dependencies were examined by the thioflavin T method. We observed that fluorescence intensity in $A\beta_{1-40}$ and $A\beta_{1-42}$ declined in a concentration-dependent manner (Fig. 1a and b). $A\beta_{1-40}$ fibril formation was inhibited by 10 μg/mL of the water (48.5 ± 0.3%), methanol (40.1 ± 2.8%), and ethanol (34.6 ± 0.2%) extracts of *Paeonia suffruticosa*. $A\beta_{1-42}$ fibril formation was also inhibited by each of the three different extracts (10 μg/mL), although the inhibitory concentration was lower than for $A\beta_{1-40}$.

In the analysis of fibril destabilization, fluorescence derived from thioflavin T was decreased in a dose-dependent manner after the addition of each of the extracts of *Paeonia suffruticosa* to pre-formed Aβ fibrils, and the degree of inhibition was similar to that observed on Aβ aggregation (Fig. 1c and d). Pre-formed $A\beta_{1-40}$ fibrils were destabilized by 10 μg/mL of the water (58.2 ± 3.7%), methanol (74.9 ± 1.1%) and ethanol (71.7 ± 1.0%) extracts. Over 80% of pre-formed $A\beta_{1-40}$ and $A\beta_{1-42}$ fibrils were destabilized by each of the three different extracts at the concentration of 100 μg/mL.

Step-through passive-avoidance tests

Step-through passive-avoidance tests were carried out in Tg2576 mice at 11 to 14 months of age. In the first acquisition trial of the learning stage, all mice (11 months

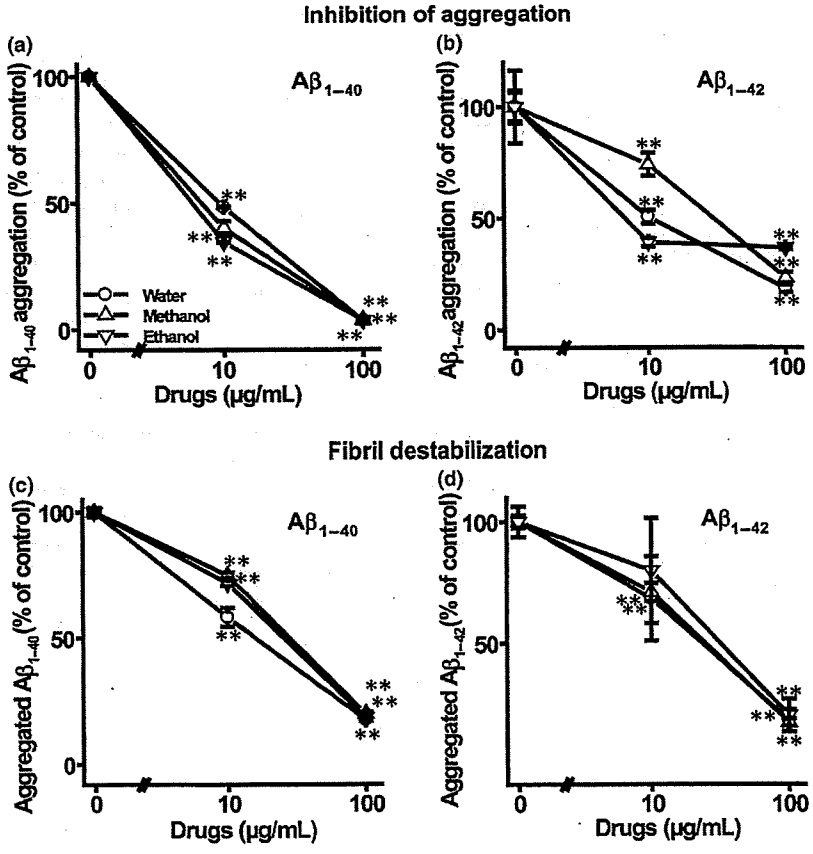

Fig. 1 Effects of three different *Paeonia suffruticosa* extracts on the kinetics of Aβ formation and destabilization. a and b: Aβ aggregate-formation assay. Reaction mixtures containing 20 μM of $A\beta_{1-40}$ (a) or $A\beta_{1-42}$, (b) 50 mM phosphate buffer (pH 7.4), and various extracts [water (circles), methanol (upward-pointing triangles), and ethanol (downward-pointing triangles)] were incubated at 37°C for 96 h (a) or 24 h (b). Aβ aggregation was expressed as percentage of the control sample which did not contain herbal extract. c and d: Aβ aggregate-destabilization assay. Reaction mixtures containing 20 μM $A\beta_{1-40}$ (c) or $A\beta_{1-42}$ (d) were incubated at 37°C for 96 h (c) or 24 h (d). The extracts were then added and incubated for another 30 min. Aβ aggregation was assessed by the thioflavin T method and expressed as the percentage of control aggregation in the absence of herbal extract. Values represent mean ± SD from four independent experiments. $^{**}p < 0.01$ compared with extract-untreated control.

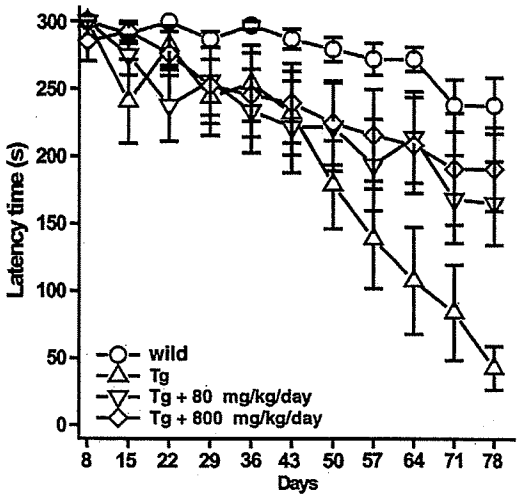

Fig. 2 Step-through latencies in the retention stages of the passive-avoidance task in *Paeonia suffruticosa*-treated transgenic (Tg2576) mice. Wild type and transgenic mice could acquire the avoidance memory by four or five repeated learning trials. The retention trials were carried out once per week for 10 weeks from Days 8 to 78 to evaluate the retention of avoidance memory. The latency time was measured for up to 300 s without delivering foot-shock. Wild type (Wild: circles); transgenic mice (Tg: upward-pointing triangles); 80 mg/kg/day *Paeonia suffruticosa* by repeated oral administration (Tg + 80 mg/kg/day: downward-pointing triangles), and 800 mg/kg/day *Paeonia suffruticosa* (Tg + 800 mg/kg/day: diamond). Values represent the means ± SD from 11 to 17 independent experiments.

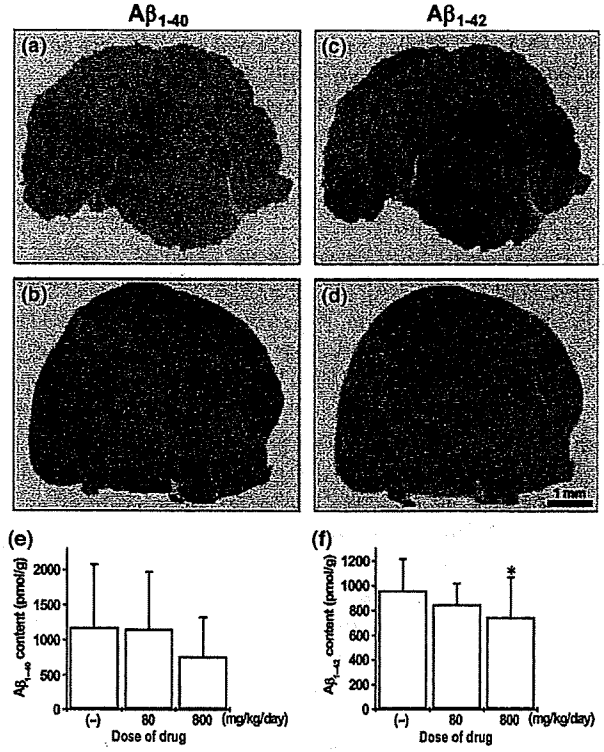

Fig. 3 Immunostaining (a–d) and ELISA analysis of formic acid-extractable Aβ levels (e and f) after dietary intake of *Paeonia suffruticosa* in Tg2576 mice. (a–d) Hemibrain cryostat sections were labeled with anti-$A\beta_{1-40}$ (a and b) and $A\beta_{1-42}$ (c and d) antibody. Image analysis was performed on the cerebral cortex from untreated (a and c) and *Paeonia suffruticosa*-treated (b and d) animals. Scale bar = 1 mm. Levels of $A\beta_{1-40}$ (e) and $A\beta_{1-42}$ (f) were quantified using an ELISA kit on formic acid-extractable Aβ from cortices of the low intake group (80 mg/kg/day) and high intake group (800 mg/kg/day). Values represent mean ± SD from 11 to 17 independent experiments. $^*p < 0.05$ compared with *Paeonia suffruticosa*-untreated control.

old) in the wild type and Tg groups entered the dark compartment immediately after being placed in the illuminated compartment. Repeating the acquisition trial increased the latency times in both groups. All mice in the wild type and Tg groups acquired avoidance memory, staying in the illuminated compartment for over 300 s on the fifth acquisition day. However, no significant differences were observed in the mean latency times between the wild type and Tg groups on any given day during the learning stage (data not shown). In retention trials (Fig. 2), the step-through latency of the Tg group was significantly reduced when compared with that of the wild type group. *Paeonia suffruticosa*-treated Tg mice were indistinguishable from non-transgenic littermates on days from 50 to 78 of testing.

Aβ pathology was reduced in *Paeonia suffruticosa*-treated Tg mice

To determine whether oral *Paeonia suffruticosa* treatment affected the accumulation of Aβ in brain tissue, we evaluated Aβ immunoreactivity in brain sections from untreated (Fig. 3a and c) and *Paeonia suffruticosa*-treated mice (Fig. 3b and d) using BA27 and BC05 antibodies which recognize the C-terminus of human $A\beta_{1-40}$ (Fig. 3a and b) and $A\beta_{1-42}$ (Fig. 3c and d). The number of Aβ-positive spots in the cortex and hippocampus were obviously lower in the *Paeonia suffruticosa*-treated mice compared with the untreated mice. No Aβ immunoreactivity was observed in brain sections from non-transgenic mice (data not shown).

We next measured the levels of $A\beta_{1-40}$ and $A\beta_{1-42}$ in brain tissue samples from Tg mice using a sensitive ELISA method (Fig. 3e and f). Consistent with the results of Aβ immunostaining, the $A\beta_{1-42}$ concentration in the samples from *Paeonia suffruticosa*-treated Tg mice (800 mg/kg/day) was significantly lower than the concentration in *Paeonia suffruticosa*-untreated mice (747.8 ± 322.4%, $p < 0.05$). In contrast to its effect on $A\beta_{1-42}$ levels, *Paeonia suffruticosa* treatment had no significant effect on $A\beta_{1-40}$ levels in the Tg mice. The levels of $A\beta_{1-40}$ and $A\beta_{1-42}$ were below the limit of detection in cerebral cortex samples from non-transgenic mice (data not shown).

HPLC analyses of *Paeonia suffruticosa*: identification of four different natural compounds and their effects on the kinetics of $A\beta_{1-42}$ formation and destabilization

The three-dimensional-HPLC fingerprints of water extracts of *Paeonia suffruticosa* are illustrated in Fig. 4. The water extract contained several different chemical compounds including paeonol, benzoic acid, and derivatives of paeoniflorin as well as PGG.

Concentration dependence of the inhibitory effects of these compounds on Aβ fibril formation was examined using the thioflavin T method (Fig. 5a). Only PGG induced a concentration-dependent decline in the thioflavin T fluorescence intensity associated with $A\beta_{1-42}$. PGG (3 μM) inhibited $A\beta_{1-42}$ fibril formation by more than 50%. Additional thioflavin-T experiments were performed in order to determine the ability of PGG to destabilize pre-formed Aβ fibrils. Fluorescence derived from thioflavin T was decreased in a dose-dependent manner after the addition of PGG to pre-formed Aβ fibrils to an extent similar to that seen for the inhibition of Aβ aggregation (Fig. 5b).

Next, we incubated different concentrations of PGG with unpolymerized $A\beta_{1-42}$ (10 μM) and monitored the formation of amyloid using the Thioflavin T method (Fig. 6). In the absence of PGG, $A\beta_{1-42}$ formed Thioflavin T-binding aggregates after a lag phase of 2 h, whereas thioflavin T signals were decreased to 33.6 ± 16.8% by 1 μM PGG after a lag phase of 24 h. Moreover, $A\beta_{1-42}$ aggregation was completely inhibited by 100 μM PGG.

Effect of PGG on $A\beta_{1-42}$ oligomers

To further characterize the breakdown products that accumulated in the presence of PGG, aliquots of $A\beta_{1-42}$ oligomerization reaction mixtures in the presence or absence of PGG were assayed by flow cytometric analysis (Fig. 7). In the absence of PGG, the fluorescence intensity of $A\beta_{1-42}$ oligomerized sample was potent compared with vehicle sample without $A\beta_{1-42}$ oligomers (Fig. 7a and b). Samples treated with PGG reduced the fluorescence intensity in a concentration-dependent manner (Fig. 7c–e). These data confirmed that PGG was a strong inhibitor of $A\beta_{1-42}$ oligomerization.

Neuroprotective effects of PGG against Aβ toxicity

To evaluate whether PGG could potentially prevent Aβ-induced toxicity, we pre-incubated SK-N-SH cells for 30 min with PGG, followed by 24 h treatment with 10 μM aggregated $A\beta_{1-42}$. SK-N-SH cell viability was significantly impaired by Aβ peptides, measured by MTT assay. PGG (10 μM) significantly protected SK-N-SH cells against Aβ-induced toxicity. When measured by MTT reduction, cell survival was restored from 56.9 ± 2.5% to 87.0 ± 13.6% in response to the $A\beta_{1-42}$ aggregates (Fig. 8).

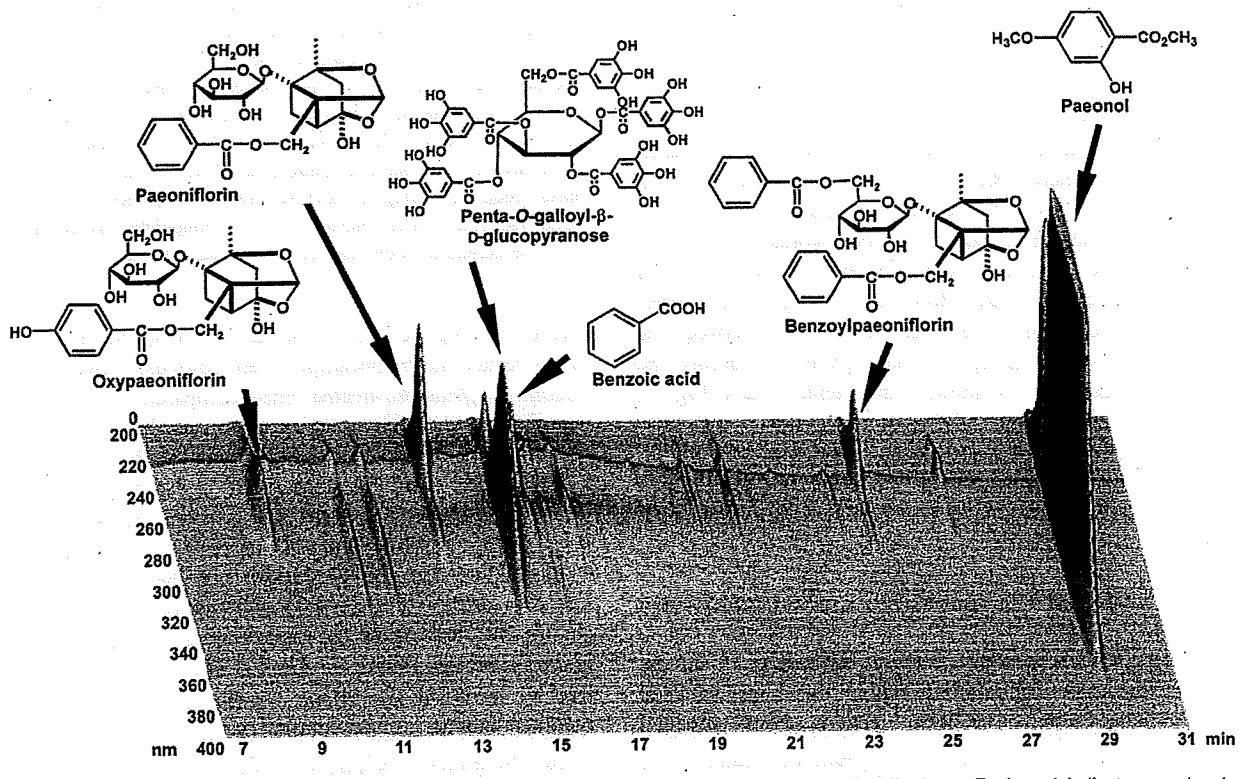

Fig. 4 Identification of chemicals by three-dimensional HPLC analysis of the water extract of *Paeonia suffruticosa*. Each peak indicates a molecule described in the figure.

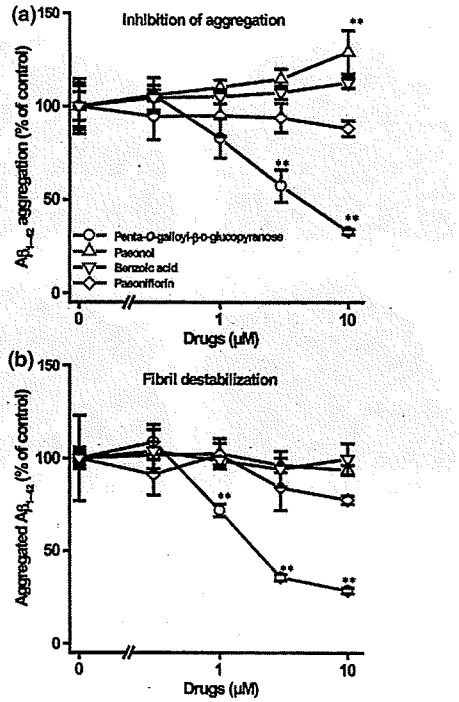

Fig. 5 Effects of distinct compounds isolated from *Paeonia suffruticosa* on the kinetics of Aβs formation and destabilization. a: Aβ aggregate-formation assay. Reaction mixtures containing 20 μM of $A\beta_{1-42}$, 50 mM phosphate buffer (pH 7.4), and various compounds [1,2,3,4,6-penta-*O*-galloyl-β-D-glucopyranose (circles), paeonol (upward-pointing triangles), benzoic acid (downward-pointing triangles), and paeoniflorin (diamond)] were incubated at 37°C for 24 h. Aβ aggregation is expressed as percentage of control observed in the absence of test compounds. b: Aβ aggregate-destabilization assay. Reaction mixtures containing 20 μM $A\beta_{1-42}$ were incubated at 37°C for 24 h. The extracts were added and incubated for 30 min. Aβ aggregation was assessed by the thioflavin T method and expressed as percentage of control aggregation observed in the absence of test compounds. Values represent mean ± SD from four independent experiments. $^{**}p < 0.01$ compared with extract-untreated control.

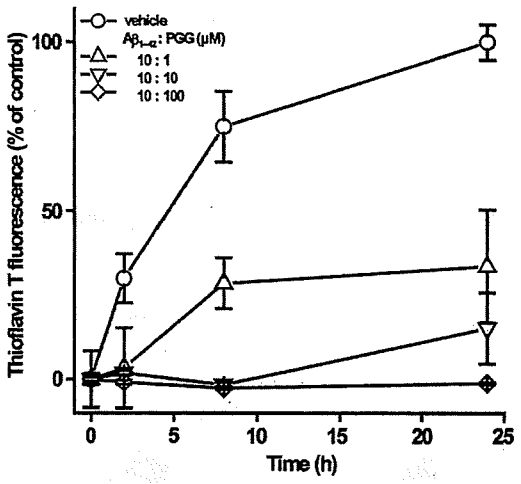

Fig. 6 The molar ratio of the Aβ–PGG interaction. Reaction mixtures containing 10 μM $A\beta_{1-42}$: PGG [solvent alone (circles), molar ratio 10 : 1 (upward-pointing triangles), 10 : 10 (downward-pointing triangles), and 10 : 100 (diamond)] were incubated at 37°C for indicated time. Thioflavin T fluorescence was expressed as a percentage of control which was observed at the point of 24 h without PGG. Values represent mean ± SD from four independent experiments.

Aβ pathology is diminished in PGG-treated Tg mice

To determine the effect of oral PGG treatment accumulation of Aβ in Tg type mice, we evaluated Aβ immunoreactivity in brain sections from untreated and PGG-treated mice by using antibodies BA27 and BC05 (Fig. 9a–d). The number of Aβ-positive spots in the hippocampus was obviously lower in PGG-treated mice (Fig. 9b and d) compared with untreated mice (Fig. 9a and c). No Aβ immunoreactivity was observed in brain sections from non-transgenic mice (data not shown).

We next measured the levels of $A\beta_{1-40}$ and $A\beta_{1-42}$ in brain samples from Tg mice by using a sensitive ELISA method (Fig. 9e and f). In the brains of Tg mice treated with PGG by repeated oral administration, the $A\beta_{1-40}$ and $A\beta_{1-42}$ concentrations were significantly lower (2417.5 ± 279.5% and 46.8 ± 3.0%, $p < 0.01$) than those in PGG-untreated mice. The levels of $A\beta_{1-40}$ and $A\beta_{1-42}$ were below the limit of detection in cerebral cortex samples from non-transgenic mice (data not shown).

Discussion

In AD research, much attention has focused on altering the course of the disease through early diagnosis and intervention. Clinical application of biomarkers and amyloid imaging may be attractive and realistic diagnostic procedures by which to identify the disease early. On the other hand, safety is an important concern with regard to early intervention with disease modifying drugs. *Paeonia suffruticosa* has been used medicinally in humans for more than 1000 years with virtually no toxic effects reported.

The results of our studies using thioflavin T fluorescence demonstrated that *Paeonia suffruticosa* extracts, regardless of the extraction method used, could inhibit the assembly of Aβ fibrils. All three extracts (water, methanol, and ethanol) induced a dramatic decline in the fluorescence intensity of thioflavin T in the μg/mL range. In our preliminary experiment, we confirmed that these extracts did not quench thioflavin T fluorescence at the indicated concentrations. These results suggest two possibilities; one is that *Paeonia suffruticosa* indeed destabilizes Aβ fibrils, and the other is that it antagonizes the binding of thioflavin T to Aβ. It has been reported that absorbance of Congo red was increased by binding to Aβ protein as well as to thioflavin T. The binding site in Aβ to Congo red was different from that to thioflavin

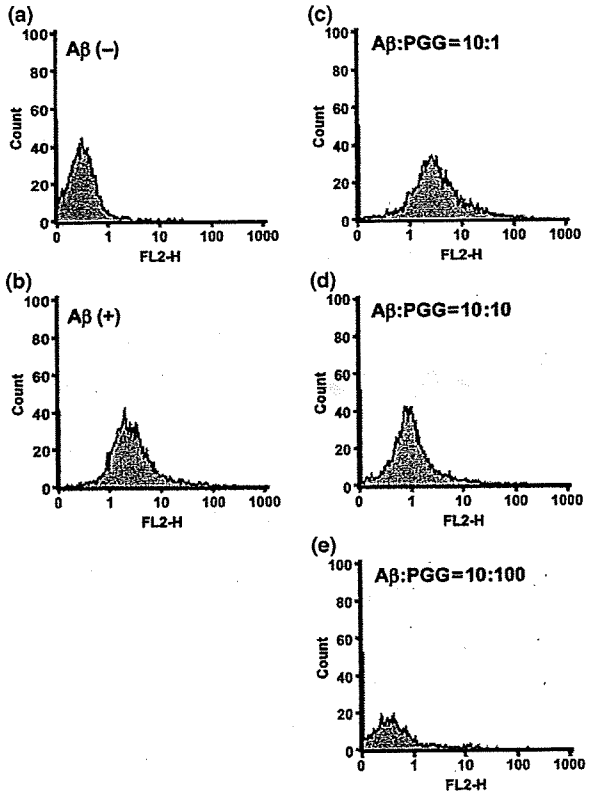

Fig. 7 Effects of PGG on $A\beta_{1-42}$ oligomeric species. These histograms were developed using reagents provided in the Aggregated Aβ Assay Kit. a: buffer-control; b: 10 μM $A\beta_{1-42}$ in absent of PGG; c–e: 10 μM $A\beta_{1-42}$ with PGG molar ratio 10 : 1 (c), 10 : 10 (d), and 10 : 100 (e).

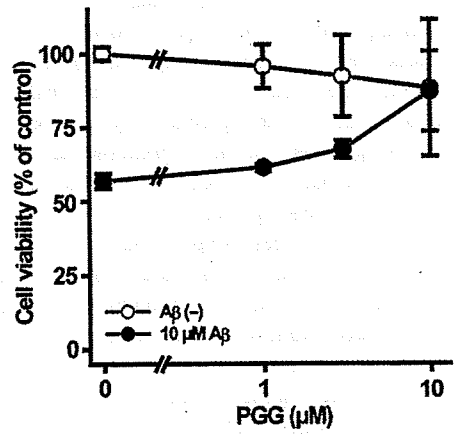

Fig. 8 Effects of PGG against Aβ-induced toxicity. SK-N-SH cells were pre-treated without or with PGG for 30 min followed by incubation without or with $A\beta_{1-42}$ (10 μM) for 24 h. Cell viability was assessed by MTT method and expressed as a percentage of control viability, which was observed in the absence of $A\beta_{1-42}$ and PGG. Values represent the means ± SD from four independent experiments.

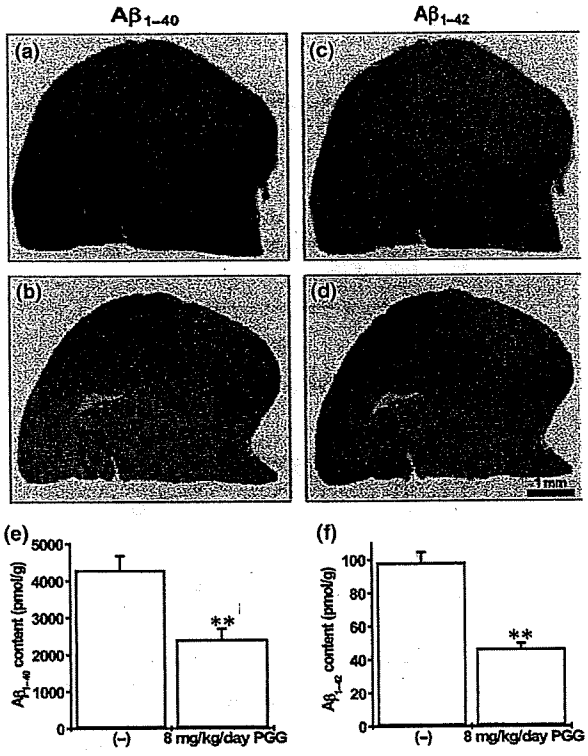

Fig. 9 Immunostaining (a–d) and ELISA analysis of formic acid-extractable Aβ levels (e and f) after dietary intake of 1,2,3,4,6-penta-*O*-galloyl-β-D-glucopyranose (PGG) in Tg2576 mice. (a–d) Hemibrain cryostat sections were labeled with anti- $A\beta_{1-40}$ (a and b) and $A\beta_{1-42}$ (c and d) antibody. Image analysis was performed on the cerebral cortices from PGG-untreated (a and c) and -treated (b and d) animals. Scale bar = 1 mm. Levels of $A\beta_{1-40}$ (e) and $A\beta_{1-42}$ (f) were quantified on formic acid-extractable Aβ from cortices of the 8 mg/kg/day PGG groups. Values represent mean ± SD from seven to eight independent experiments. $^{**}p < 0.01$, compared with PGG-untreated control.

T. In our experiments, each of the three *Paeonia suffruticosa* extracts decreased the absorbance of Congo red (data not shown), suggesting that the decrease in thioflavin T fluorescence by *Paeonia suffruticosa* extracts was caused by destabilization of Aβ fibrils. Moreover, our preliminary atomic force microscopy data also strongly support this notion, as destabilization of Aβ fibrils by *Paeonia suffruticosa* extracts was directly visualized (data not shown). The extracts of *Paeonia suffruticosa* inhibited aggregation of both $A\beta_{1-40}$ and $A\beta_{1-42}$ to a similar extent. Therefore, the inhibitory effect of *Paeonia suffruticosa* on amyloidogenesis of Aβ may not be dependent on the distinct amino acid sequence of its C-terminal.

Paeonia suffruticosa treatment prevented Aβ-related memory deficits and AD-type neuropathology *in vivo*. In our study, we found that treatment of Tg2576 mice with *Paeonia suffruticosa* attenuated memory deterioration, and this effect coincided with an approximately 20% reduction in

Aβ peptide content in the brain. We hypothesize that treatment with *Paeonia suffruticosa* may have beneficial effects on AD-type memory deterioration through a direct interaction between *Paeonia suffruticosa* and Aβ peptides in the brain, leading to the prevention of Aβ plaque formation.

Our studies also showed that PGG at low concentrations ($IC_{50} = 3$ μM) can inhibit Aβ aggregation or promote its destabilization. Moreover, our preliminary scanning electron microscopy data also strongly support this notion, as destabilization of Aβ fibrils by PGG was directly visualized (Fig. S1). As other chemical compounds, such as paeonol, benzoic acid, and paeoniflorin had no effects on Aβ aggregation, PGG may be the principal active constituent responsible for the effect of *Paeonia suffruticosa* on Aβ fibril regulation. Previous published literatures reported that several polyphenols, such as those from green tea or grape, had anti-aggregation property (Ehrnhoefer *et al.* 2008; Rivière *et al.* 2008). PGG had a comparable inhibitory effect with such published polyphenols.

The toxicity of Aβ is becoming more strongly linked to the formation of oligomeric aggregates (Kirkitadze *et al.* 2002). In our experiments, PGG inhibited Aβ oligomerization. Moreover, treatment of SK-N-SH cells with PGG significantly protected the cells from $Aβ_{1-42}$ toxicity at concentrations similar to those that inhibited Aβ aggregation. Thus, our experiments suggest that PGG inhibited not only Aβ fibril formation but also neurotoxic Aβ oligomer formation. Furthermore, oral intake of PGG reduced Aβ plaque burden and Aβ peptide content in brain tissue from Tg2576 mice, as did like *Paeonia suffruticosa*. There are two possible explanations; one is that PGG indeed destabilizes Aβ fibrils, and the other is that it inhibits the Aβ production or its secretion in Tg2576 mice brain. We demonstrated that PGG did not affect the level of full-length APP in Tg2576 mice (Figure S2), suggesting that the decrease in Aβ plaques and Aβ peptide content in brain tissue from Tg2576 mice by PGG may be caused by destabilization of Aβ fibrils. Curcumin, an active compound of *Curcuma longa*, was reported to inhibit Aβ fibril formation and to destabilize preformed Aβ fibrils *in vitro* and *in vivo* (Ono *et al.* 2004; Yang *et al.* 2005). It has also been reported that this compound is highly hydrophobic and should readily enter the brain to bind to plaques *in vivo* (Yang *et al.* 2005). Although highly hydrophilic, unlike curcumin, PGG has curcumin-like activity on Aβ fibril regulation *in vivo*. Studies of the metabolism of PGG and its ability to penetrate the blood-brain barrier by this compound are now underway.

In conclusion, our study demonstrates that *Paeonia suffruticosa* and PGG not only inhibit Aβ fibril formation but also disassemble pre-formed Aβ fibrils. Moreover, our experiments suggest that PGG inhibits Aβ oligomerization and Aβ toxicity. As a result, it improved memory deficits in Tg2576 mice. Therefore, extracts of *Paeonia suffruticosa* and PGG could have potential as therapeutic drugs for AD patients and may also be useful as primary or secondary preventive agents for healthy individuals and patients with mild cognitive impairment. Furthermore, *Paeonia suffruticosa* has a satisfactory safety profile because no obvious adverse effects of *Pilulae octo-medicamentorum rehmanniae* have been reported. In our preliminary experiments, *Paeonia suffruticosa* was tested for hepatotoxicity, nephrotoxicity, and other biochemical parameters in transgenic mice. Fortunately, this medicinal herb did not show any signs of organ toxicity. Thus, *Paeonia suffruticosa* appears to be a safe natural product for regulating Aβ aggregation. *Paeonia suffruticosa* and PGG may represent a new class of therapeutic and preventive agents for AD which act to regulate the formation and the clearance of senile plaques.

Acknowledgements

This work was partially supported by (i) a grant-in-aid for scientific research from the Ministry of Education, Science, Sports and Culture of Japan (#16590554), (ii) a program for the promotion of fundamental studies in Health Science of the National Institute of Biomedical Innovation (NIBIO) of Japan (#03-1), and (iii) a grant-in-aid from Core Research for Evolutional Science and Technology of Japan Science and Technology Corporation. We thank S. Isogami and M. Takahashi for kind advice and technical supports.

Supporting Information

Additional Supporting Information may be found in the online version of this article:

Figure S1 Scanning electron microscope imaging of $Aβ_{1-42}$ fibrils. After incubation of $Aβ_{1-42}$ for 24 h for preformed fibrils, the mixture of aggregated Aβ and the PGG was incubated at 37°C for 1 h. A: vehicle (DMSO); B: 10 μM $Aβ_{1-42}$: 10 μM PGG (molar ratio 1 : 1). Scale bar = 5 μm.

Figure S2 Effects of PGG on the level of amyloid precursor protein (APP) in Tg2576 mice. Immunoblotting of brain levels of APP after dietary 1,2,3,4,6-penta-*O*-galloyl-β-D-glucopyranose (PGG) in Tg2576. Levels of APP were quantitated by immunoblotting with full length APP antibody from cortices of 8 mg/kg/day-PGG groups. The samples were separated on a 10% polyacrylamide gel, followed by immunoblotting with anti-full length APP antibody. Arrowheads point to APP. Similar results were obtained from at least 3 independent experiments.

Please note: Wiley-Blackwell are not responsible for the content or functionality of any supporting materials supplied by the authors. Any queries (other than missing material) should be directed to the corresponding author for the article.

References

Anderton B. H., Callahan L., Coleman P. *et al.* (1998) Dendritic changes in Alzheimer's disease and factors that may underlie these changes. *Prog. Neurobiol.* **55**, 595–609.

Barghorn S., Nimmrich V., Striebinger A. *et al.* (2005) Globular amyloid beta-peptide oligomer – a homogenous and stable neuropathological protein in Alzheimer's disease. *J. Neurochem.* **95**, 834–847.

Barrow C. J. and Zagorski M. G. (1991) Solution Structures of β-peptide and its constituent fragments: relation to amyloid deposition. *Science* **253**, 179–182.

Calon F., Lim G. P., Yang F. *et al.* (2004) Docosahexaenoic acid protects from dendritic pathology in an Alzheimer's disease mouse model. *Neuron* **43**, 633–645.

Chou T. C. (2003) Anti-inflammatory and analgesic effects of Paeonol in carrageenan-evoked thermal hyperalgesia. *Br. J. Pharmacol.* **139**, 1146–1152.

Darreh-Shori T., Hellstrom-Lindahl E., Flores-Flores C. *et al.* (2004) Long-lasting acetylcholinesterase splice variations in anticholinesterase-treated Alzheimer's disease patients. *J. Neurochem.* **88**, 1102–1113.

Ehrnhoefer D. E., Bieschke J., Boeddrich A. *et al.* (2008) EGCG redirects amyloidogenic polypeptides into unstructured, off-pathway oligomers. *Nat. Struct. Mol. Biol.* **15**, 558–566.

Fujiwara H., Iwasaki K., Furukawa K. *et al.* (2006) *Uncaria rhynchophylla*, a Chinese medicinal herb, has potent antiaggregation effects on Alzheimer's beta-amyloid proteins. *J. Neurosci. Res.* **84**, 427–433.

Hofmann T., Glabasnia A., Schwarz B. *et al.* (2006) Protein binding and astringent taste of a polymeric procyanidin, 1,2,3,4,6-penta-*O*-galloyl-beta-D-glucopyranose, castalagin, and grandinin. *J. Agric. Food. Chem.* **54**, 9503–9509.

Hsieh C. L., Cheng C. Y. and Tsai T. H. (2006) Paeonol reduced cerebral infarction involving the superoxide anion and microglia activation in ischemia-reperfusion injured rats. *J. Ethnopharmacol.* **106**, 208–215.

Iwasaki K., Kobayashi S., Chimura Y. *et al.* (2004) A randomized, double-blind, placebo-controlled clinical trial of the Chinese medicinal herb "ba wei di huang wan" in the treatment of dementia. *J. Am. Geriatr. Soc.* **52**, 1518–1521.

Iwasaki K., Satoh-Nakagawa T., Maruyama M. *et al.* (2005) A randomized, observer-blind, controlled trial of the traditional Chinese medicine Yi-Gan San for improvement of behavioral and psychological symptoms and activities of daily living in dementia patients. *J. Clin. Psychiatry* **66**, 248–252.

Kirkitadze M. D., Bitan G. and Teplow D. B. (2002) Paradigm shifts in Alzheimer's disease and other neurodegenerative disorders: the emerging role of oligomeric assemblies. *J. Neurosci. Res.* **69**, 567–577.

Le Bars P. L., Katz M. M., Berman N. *et al.* (1997) A placebo-controlled, double-blind, randomized trial of an extract of Ginkgo biloba for dementia. North American EGb Study Group. *JAMA* **278**, 1327–1332.

Li Y., Kim J., Li J. *et al.* (2005) Natural anti-diabetic compound 1,2,3,4,6-penta-*O*-galloyl-D-glucopyranose binds to insulin receptor and activates insulin-mediated glucose transport signaling pathway. *Biochem. Biophys. Res. Commun.* **336**, 430–437.

Lin H. C., Ding H. Y., Ko F. N. *et al.* (1999) Aggregation inhibitory activity of minor acetophenones from *Paeonia* species. *Planta Med.* **65**, 595–599.

Millard C. B. and Broomfield C. A. (1995) Anticholinesterases: medical applications of neurochemical principles. *J. Neurochem.* **64**, 1909–1918.

Nakagawasai O., Yamadera F., Iwasaki K. *et al.* (2004) Effect of kami-untan-to on the impairment of learning and memory induced by thiamine-deficient feeding in mice. *Neuroscience* **125**, 233–241.

Ono K., Hasegawa K., Naiki H. *et al.* (2004) Curcumin has potent anti-amyloidogenic effects for Alzheimer's beta-amyloid fibrils in vitro. *J. Neurosci. Res.* **75**, 742–750.

Park C. H., Lee Y. J., Lee S. H. *et al.* (2000) Dehydroevodiamine HCl prevents impairment of learning and memory and neuronal loss in rat models of cognitive disturbance. *J. Neurochem.* **74**, 244–253.

Rivière C., Richard T., Vitrac X. *et al.* (2008) New polyphenols active on beta-amyloid aggregation. *Bioorg. Med. Chem. Lett.* **18**, 828–831.

Selkoe D. J. (2002) Alzheimer's disease is a synaptic failure. *Science* **298**, 789–791.

Suemoto T., Okamura N., Shiomitsu T. *et al.* (2004) *In vivo* labeling of amyloid with BF-108. *Neurosci. Res.* **48**, 65–74.

Suzuki T., Arai H., Iwasaki K. *et al.* (2001) A Japanese herbal medicine (Kami-Untan-To) in the treatment of Alzheimer's disease: A pilot study. *Alzheimer's Rep.* **4**, 177–182.

Tierney M. C., Fisher R. H., Lewis A. J. *et al.* (1988) The NINCDS-ADRDA Work Group criteria for the clinical diagnosis of probable Alzheimer's disease: a clinicopathologic study of 57 cases. *Neurology* **38**, 346–359.

Wirths O., Multhaup G. and Bayer T. A. (2004) A modified β-amyloid hypothesis: intraneuronal accumulation of the β-amyloid peptide – the first step of a fatal cascade. *J. Neurochem.* **91**, 513–520.

Yang F., Lim G. P., Begum A. N. *et al.* (2005) Curcumin inhibits formation of amyloid beta oligomers and fibrils, binds plaques, and reduces amyloid in vivo. *J. Biol. Chem.* **280**, 5892–5901.

Yasuda T., Kon R., Nakazawa T. *et al.* (1999) Metabolism of Paeonol in rats. *J. Nat. Prod.* **62**, 1142–1144.

Neurobiology of Disease 36 (2009) 259–268

Contents lists available at ScienceDirect

Neurobiology of Disease

journal homepage: www.elsevier.com/locate/ynbdi

CREB is a key regulator of striatal vulnerability in chemical and genetic models of Huntington's disease

Yun-Sik Choi [a], Boyoung Lee [a], Hee-Yeon Cho [a], Iza B. Reyes [a], Xin-An Pu [b], Takaomi C. Saido [c], Kari R. Hoyt [d,*], Karl Obrietan [a,*]

[a] Department of Neuroscience, Ohio State University, Columbus, OH 43210, USA
[b] Center for Molecular Neurobiology, Ohio State University, Columbus, OH 43210, USA
[c] Chemical Neuroscience Group 2-1, RIKEN Brain Science Institute, Saitama 351-0198, Japan
[d] Division of Pharmacology, Ohio State University, Columbus, OH 43210, USA

ARTICLE INFO

Article history:
Received 8 April 2009
Revised 26 June 2009
Accepted 15 July 2009
Available online 24 July 2009

Keywords:
Huntington's
CREB
3-NP
Mouse
Transgenic
Striatum

ABSTRACT

Evidence of dysregulation of the CREB/CRE transcriptional pathway in animal models of Huntington's disease (HD) suggests that strategies designed to augment CRE-mediated transcription may be of therapeutic value. Here, we investigated the consequences of CREB activation and repression in chemical and transgenic mouse models of HD. In the 3-nitropropionic acid (3-NP) model, CREB phospho-activation in the striatum was potently repressed within the neurotoxic "core" region prior to cell death. Conversely, marked expression of phospho-CREB, as well the CREB-regulated cytoprotective gene Bcl-2, was detected in the "penumbral" region. To examine potential contributory roles for the CREB/CRE transcriptional pathway in striatal degeneration, we used both CREB loss- (A-CREB) and gain- (VP16-CREB) of-function transgenic mouse strains. 3-NP-induced striatal lesion size and motor dysfunction were significantly increased in A-CREB mice compared to controls. Conversely, striatal damage and motor deficits were diminished in VP16-CREB mice. Furthermore, transgenic A-CREB significantly accelerated motor impairment in the YAC128 mouse model of HD. Together, these results indicate that CREB functionality is lost during the early stages of striatal cell stress and that the repression of CREB-mediated transcription contributes to the pathogenic process.

Introduction

Huntington's disease (HD) is a neurodegenerative disorder characterized by striatal and cortical atrophy, and a typical onset of motor and cognitive symptoms in midlife (reviewed in Gil and Rego, 2008). HD is an autosomal dominant genetic disease caused by a poly-glutamine repeat size greater than 35 in the huntingtin protein (reviewed in Semaka et al., 2006). Both the normal function of huntingtin and the mechanism of toxicity of poly-glutamine expanded huntingtin are yet to be definitively established. However, transcriptional dysregulation, excitotoxicity, oxidative stress, mitochondrial dysfunction, disruption of axonal transport and synaptic dysfunction have all been implicated in HD-induced neuronal dysfunction and death (Cha, 2007; reviewed in Roze et al., 2008b). Given that many of these pathophysiological processes likely result from HD-evoked alterations in transcriptional networks, an understanding of the underlying cellular signaling state of the distressed striatum is merited.

In this regard, a particularly interesting set of observations has shown that HD pathogenesis leads to dysregulation of the CREB/cAMP response element (CRE) transcriptional pathway (Cui et al., 2006; DeMarch et al., 2007, 2008; Lee et al., 2005a,b; Nucifora et al., 2001; Obrietan and Hoyt, 2004). CREB is a member of the basic leucine zipper family of transcription factors and plays diverse roles in an array of physiological processes (Huang et al., 2008; Krönke et al., 2003; Marie et al., 2005; Redmond et al., 2002; Shieh et al., 1998; Suzuki et al., 2007; Tao et al., 1998; Wilson et al., 1996). Within the nervous system, CREB regulates a wide range of neuroprotective processes, including the expression of trophic factors, antiapoptotic genes, detoxifying enzymes, and mitochondrial biogenesis (Shieh et al., 1998; Tao et al., 1998; St. Pierre et al., 2006; Wilson et al., 1996). Therefore, manipulation of the CREB/CRE transcriptional pathway represents a promising target for amelioration of HD pathology.

To begin our analysis of CREB and striatal cell death, we employed the YAC128 mouse strain and the 3-nitropropionic acid (3-NP) model of striatal neuron toxicity. YAC128 mice express a polyglutamine expanded form of human huntingtin and show a progressive motor deficit from 6 months of age (Slow et al., 2003). 3-NP is a potent,

* Corresponding authors. K. Obrietan is to be contacted at the Department of Neuroscience Ohio State University Graves Hall, Rm 4118, 333 W. 10th Ave. Columbus, OH 43210, USA. Fax: +1 614 688 8742. K. R. Hoyt, Division of Pharmacology, Ohio State University, Riffe Building, Rm 412, 496 W. 12th Ave. Columbus, OH 43210, USA. Fax: +1 614 292 9083.
E-mail addresses: hoyt.31@osu.edu (K.R. Hoyt), obrietan.1@osu.edu (K. Obrietan).
Available online on ScienceDirect (www.sciencedirect.com).

0969-9961/$ – see front matter © 2009 Elsevier Inc. All rights reserved.
doi:10.1016/j.nbd.2009.07.014

irreversible, mitochondrial toxin that triggers a marked reduction in ATP production and the rapid appearance of striatal lesions (Beal et al., 1993). The lesions are similar to those seen in HD and thus, 3-NP has been used to model HD pathology (Saulle et al., 2004) and test potential therapeutics. To investigate the role of CREB in HD pathology, and to assess the potential neuroprotective effects of CREB activation, we generated mice transgenic for a repressive form of CREB (A-CREB) and a constitutively active form of CREB (VP16-CREB). These transgenes are highly expressed in medium spiny neurons in the striatum, a primary locus of HD pathology. Here we provide evidence that CREB is a key regulator of neuroprotection in both the chemical and genetic models of HD.

Materials and methods

Animals

The generation of the tetracycline response element (TRE)-regulated-A-CREB/GFP line was previously described by Lee et al. (2007). To generate mice transgenic for TRE-regulated VP16-CREB and enhanced green fluorescence protein (GFP), we generated a pTRE VP16-CREB/GFP expression vector. To this end, VP16-CREB was isolated from a pcDNA3 expression vector (provided by Dr. Soren Impey, Oregon Health Sciences University) via HindIII and XbaI digestion. The fragment was then blunted with Klenow and subcloned into SmaI-digested pIRES2-eGFP (Invitrogen). Primers (Forward: 5′ CGGCGCGGCCGCGCCACC**ATG**GGAGCCCGGGAGATCTGGATCTGG-3′, Reverse: 5′ CGGCGCGGCCGCTTTACTTGTACAGCTCGTCCATGCC 3′) were used to amplify VP16-CREB/IRES/eGFP. A Kozak sequence (GCCACCATGG) was added upstream of start codon (bold) of VP16 CREB to improve protein expression, and a NotI digestion site (GCGGCCGC) was added to the 5′ end to allow for facile subcloning of the construct into the pTRE-Tight vector (Clontech, Mountain View, CA, USA). Next, to release the TRE promoter, VP16-CREB/IRES/eGFP and SV 40 polyA sequence, the vector was digested with XhoI. Transgenic C57BL/6 blastocytes were generated at the Ohio State University Transgenic Facility.

A bitransgenic system was used to generate tetracycline-inducible bicistronic A-CREB/eGFP and VP16-CREB/eGFP mice. To drive transgene expression, the A-CREB/eGFP and VP16-CREB/eGFP mice were crossed with CaMKIIα promoter-tTA transgenic mice (Mayford et al., 1996). To inhibit transgene expression, doxycycline (100 mg/L) was added to the drinking water of VP16-CREB mice and WT littermates from 2 weeks of age until 1 week before 3-NP injection. YAC128 mice were acquired from Jackson Lab. To generate tri-transgenic mice for YAC128::tTA::A-CREB, male mice transgenic for YAC128 were crossed with females transgenic for tTA::A-CREB. The genotypes were determined using PCR. All experiments involving animals were approved by the Ohio State University Animal Care and Use Committee.

3-NP intoxication

3-nitropropionic acid (3-NP, Sigma, St. Louis, MO) was dissolved in saline (25 mg/mL) and passed through a 0.2-μm filter. We followed the 3-NP injection protocol described by Huang et al. (2006). Briefly, 3-NP was injected intraperitoneally twice daily for 2 days at 12 h intervals (8:00 A.M. and 8:00 P.M.) at a dose of 60 mg/kg for the first two injections and 80 mg/kg for the second two injections. Animals were maintained on a standard 12 h light/dark cycle, with lights on at 6:00 A.M.

We also verified that 3-NP-induced succinate dehydrogenase (SDH) inhibition was not altered by expression of the A-CREB or VP-16 CREB transgenes. SDH activity was measured by enzyme histochemistry of frozen coronal brain sections (12 μm-thick) from A-CREB::tTA, VP-16::tTA bitransgenic and tTA monotransgenic mice sacrificed 1 h after injection of 80 mg/kg 3-NP or saline vehicle. Brain sections were incubated at 37 °C for 2 h in 0.55 mM nitroblue tetrazolium and 0.5 mM succinate as described (Higgins et al., 1999; Tabrizi et al., 2000). Importantly, we found that there was no staining in the absence of succinate substrate or in the presence of 1 mM 3-NP added directly to the incubation solution. The optical density of the stained sections was quantified using MetaMorph software (Universal Imaging, Downingtown, PA). Striatal optical density in sections from 3-NP injected mice was reduced to 26% of saline-injected mice, indicating that the 3-NP injection paradigm potently inhibited brain SDH activity. The ratio of cortical and striatal SDH activities (optical density) was compared among 3-NP-treated tTA monotransgenic, VP-16 CREB::tTA, and A-CREB::tTA bitransgenic mice. Since CREB transgene expression is concentrated in the striatum (Figs. 4A and 7A), an effect of the transgenes on the 3-NP-evoked inhibition of SDH activity should be reflected in the SDH cortex/striatum activity ratio, relative to the ratio in tTA monotransgenic mice. The ratio (cortex/striatum) of SDH activity for tTA monotransgenic mice was 1.65 ± 0.10, VP-16 CREB::tTA mice was 1.63 ± 0.10, and A-CREB::tTA mice was 1.74 ± 0.17 (mean $\pm$ sem, $n = 3$ mice per genotype; n.s. by ANOVA). Since there were no differences in the cortex/striatum ratio among the mouse lines, we conclude that neither transgenic repression nor activation modulates the capacity of 3-NP to affect SDH activity.

Tissue processing

Mice were anesthetized with a ketamine (150 mg/kg)/xylazine (30 mg/kg) cocktail and transcardially perfused with saline, followed by 4% paraformaldehyde in 0.01 M phosphate buffered saline (PBS), pH 7.4. Brains were postfixed for 4 h and then cryoprotected in 30% sucrose in 0.01 M PBS. Sequential coronal sections (40 μm) through the striatum were prepared using a cryotome. For the measurement of striatal damage, sections were processed with cresyl violet using the labeling method described in Choi et al. (2007).

Immunohistochemistry

For immunohistochemical labeling, sections (40 μm-thick) were blocked with 10% normal goat serum or 5% normal horse serum in PBS, followed by overnight incubation (4 °C) with rabbit polyclonal anti-phospho-CREB antibody (pCREB, 1:1000; Cell Signaling Technology, Beverly, MA), rabbit polyclonal anti-GFP antibody (1:4000; acquired from Dr. Luc G. Berthiaume, University of Alberta, Canada), goat anti-Bcl-2 antibody (1:500; Santa Cruz Biotechnology, Santa Cruz, CA) or a rabbit polyclonal antibody against the N-terminal fragment of α-spectrin (1:4000, Higuchi et al., 2005). Sections were then processed using the ABC staining method (Vector Laboratories, Burlingame, CA) and nickel-intensified diaminobenzidine (DAB; Vector Laboratories) was used to visualize the signal. Photomicrographs were captured as described above.

For immunofluorescence labeling, sections were blocked with 10% normal goat serum or 5% normal horse serum in PBS, followed by overnight incubation with mouse anti-NeuN antibody (1:2000; Millipore, Billerica, MA), rabbit anti-GFP antibody (1:2000), goat anti-Bcl-2 antibody (1:500; Santa Cruz Biotechnology) or rabbit anti-pCREB antibody (1:1000; Cell Signaling Technology). Next, sections were incubated (2 h at room temperature) with secondary antibodies conjugated with Alexa 488 and/or Alexa 594 (1:1000; Invitrogen, San Diego, CA) and then mounted with Cytoseal (Richard-Allan Scientific, Kalamazoo, MI). Fluorescence images were captured using a Zeiss (Oberkochen, Germany) 510 Meta confocal microscope (2-μm-thick optical section).

Fluoro-Jade B staining

Sections (40 μm) were initially mounted on gelatin-coated slides, rehydrated and incubated in 0.06% potassium permanganate solution for 10 min. Next, the sections were incubated in 0.004% Fluoro-Jade B (Millipore, Bedford, MA) solution containing 0.1% glacial acetic acid

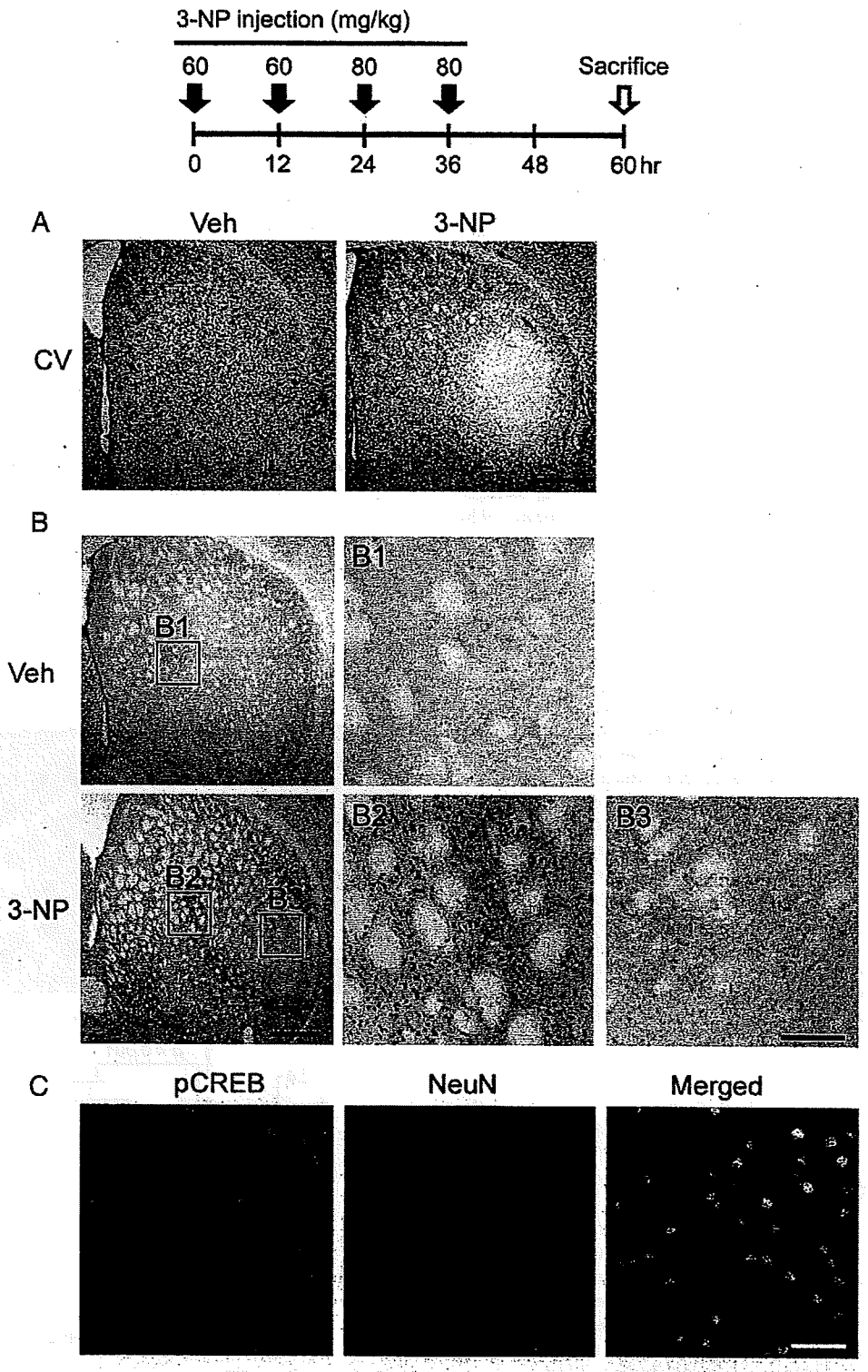

Fig. 1. 3-NP intoxication regulates striatal CREB phosphorylation. Top: Time course depicting the 3-NP injection and sacrifice schedule for experiments presented in A–C. A. Cresyl violet (CV) histology reveals marked 3-NP-induced cell damage within the lateral striatum. Tissue was collected from mice sacrificed 1 day after the last 3-NP injection. Uniform CV labeling was detected throughout the striatum of the vehicle-injected animal. Scale bar = 400 μm. B. Immunoreactivity for the Ser-133 phosphorylated form of CREB (pCREB). Top: Representative section from a vehicle-injected animal: note the modest level of pCREB expression. Boxed region (B1) is magnified to the right. Bottom: Marked pCREB expression was detected within the penumbral region (magnified in B2) surrounding the foci of 3-NP-evoked striatal damaged. Limited pCREB expression was observed within the 3-NP 'core' (magnified in B3). Scale bars: 400 μm in the low magnification image and 100 μm in the enlarged image. C. Representative immunofluorescence image within the penumbral region shows that pCREB co-labels with NeuN, indicating CREB is activated in striatal neurons. Scale bar = 50 μm.

for 20 min at room temperature, washed, and coverslipped with distrene plasticizer xylene (DPX; Electron Microscopy Sciences, Fort Washington, PA).

Measurement of striatal damage and pCREB expression

The striatal borders were defined laterally and dorsally by the corpus callosum, medially by the lateral ventricle and midline, and ventrally, by a horizontal plane through the anterior commissure. These and other neuroanatomical landmarks (as described by Fernagut et al., 2002a and Fernagut et al., 2002b) were used to ensure that consistency was maintained across all sets of animals for our analysis of 3-NP-induced striatal lesions. Analysis was performed through the rostral (bregma: +1.50 mm)- caudal (bregma: −0.50 mm) extent of the striatum. The volume of 3-NP-induced striatal damage was measured in every 5th striatal section (200 μm intervals). Photomicrographs (4×) of cresyl violet-labeled sections were captured using a 16-bit digital camera (Micromax YHS 1300; Princeton Instruments, Trenton, NJ) mounted on a Leica DM IRB microscope. For each section, the total striatal area and the damaged area (which was characterized by the extensive loss of cresyl violet signal) were digitally outlined and area measurements were calculated using MetaMorph software. Volumes were calculated by summing the cross-sectional areas in each section and the percent of striatal damage in each animal was calculated by dividing damaged volume by total striatal volume. Data are presented as the mean ± SEM, and significance was assessed using a two-tailed Student's *t*-test.

To examine activated CREB following 3-NP injection, mid-striatal (bregma +0.9 to −0.2 mm) coronal sections were immunolabeled and the pattern of pCREB expression was examined. Labeling revealed a loss of pCREB within the ostensible lesion 'core'. Both the neuroanatomical location and the size of the region demarcated by the loss of pCREB paralleled the 3-NP-evoked lesion pattern revealed using cresyl violet and Fluoro-Jade B labeling. Surrounding this was an ~300 μm zone where relatively high pCREB levels were observed: this region is referred to as the 'penubra'. Lastly, we denoted a 'medial' striatal region adjacent to the penumbra, which did not exhibit marked signs of cell stress. To quantitate pCREB levels, densitometric analysis was performed within these three regions; for the core, intensity was measured within a 200 μm digital circle placed in the center of the core; penumbra pCREB levels were determined by measuring the intensity within concentric rings that defined the inner and outer borders (300 μm) of the penumbra. Measurements within the medial striatal region were collected within a 200 μm digital circle, which was positioned next to the concentric rings. Values were corrected against background immunolabeling within the corpus callosum, and normalized to a value of 1 for the core region. Analysis was performed using MetaMorph software.

Rotarod assessments

Mice were trained on an accelerating rotarod (Columbus Instruments) with 3 trials per day for 3 consecutive days. Only mice which attained steady baseline of performance (300 s for the fall latency on the 3rd day) were used. The testing was executed from 1 day before to 3 or 4 days after the first 3-NP injection. Mice were tested three times a day with a 1 h interval between each test. YAC128::tTA::A-CREB animals were trained with 3 trials per day for 3 consecutive days (2–20 rpm) and rotarod performance was tested 3 times with 1 h interval (4–40 rpm). The longest latency to fall off the rotarod for the three daily trials was used for the analysis. Data are presented as the mean ± SEM, and significance was assessed using a two-tailed Student's *t*-test.

Primary neuronal culture/LDH release assay

Striatal tissue was dissected from Sprague–Dawley rat pups (E18–E19) and enzymatically digested into a single-cell suspension using the methods and reagents described by Lee et al. (2005a). Cells were seeded at a density of $2.2\times10^5/cm^2$ onto poly-D-lysine- (>540 kDa; Sigma) coated 24-well plates and maintained as described in Lee et al. (2005a). The LDH release assay was performed as described by Koh and Choi (1987). The value for LDH release from the vehicle-treatment condition was normalized to a value of 1. Data are presented as the mean ± SEM, and significance was assessed using a two-tailed Student's *t*-test.

Western blotting

Cultured neurons were rinsed with ice-cold PBS and then lysed in ice-cold RIPA buffer (150 mM NaCl, 50 mM Tris pH 7.4, 1 mM EDTA, 1% Triton X-100, 0.1% SDS, 5 mM NaF, 25 μM sodium vanadate supplemented with protease inhibitor cocktail: complete mini tablet, Roche Diagnostics). Protein content was determined via a Bradford assay (Bio-Rad, Hercules, CA). Twenty μg of protein was loaded onto a 10% SDS-PAGE gel, electrophoresed using standard procedures, and the protein was transblotted onto polyvinylidene fluoride (Immobilon P; Millipore). Following blocking with 10% (wt/vol) powdered milk, membranes were incubated (4 °C overnight) with rabbit anti-pCREB antibody (1:2000, Cell Signaling Technology). Samples were then incubated with an HRP-conjugated anti-rabbit IgG secondary antibody (1:2500, Perkin-Elmer, Wellesley, MA) and the signal was

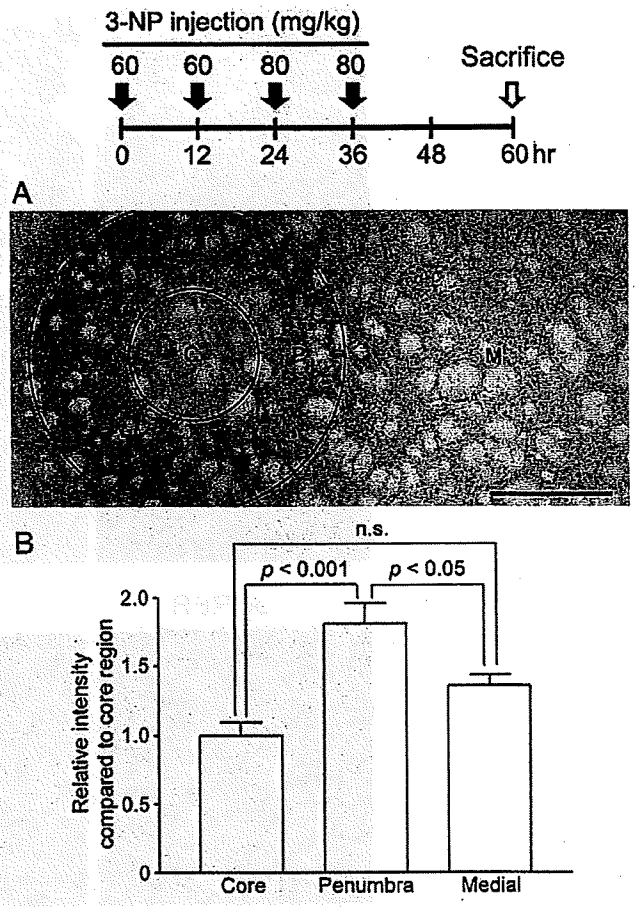

Fig. 2. 3-NP-induced pCREB in the striatum. Top) Time course depicting the 3-NP injection and sacrifice schedule. A. Concentric rings are used to depict the 3-NP-induced pattern of CREB phosphorylation within the core (C), penumbral (P) and medial (M) striatal regions. Scale bar: 400 μm. B. Quantitative densitometric analysis of pCREB expression within the 3 regions. pCREB levels were significantly higher in the penumbra than in either the core or medial regions. Data were acquired from 7 animals. *p* values were generated using the two-tailed Student's *t*-test.

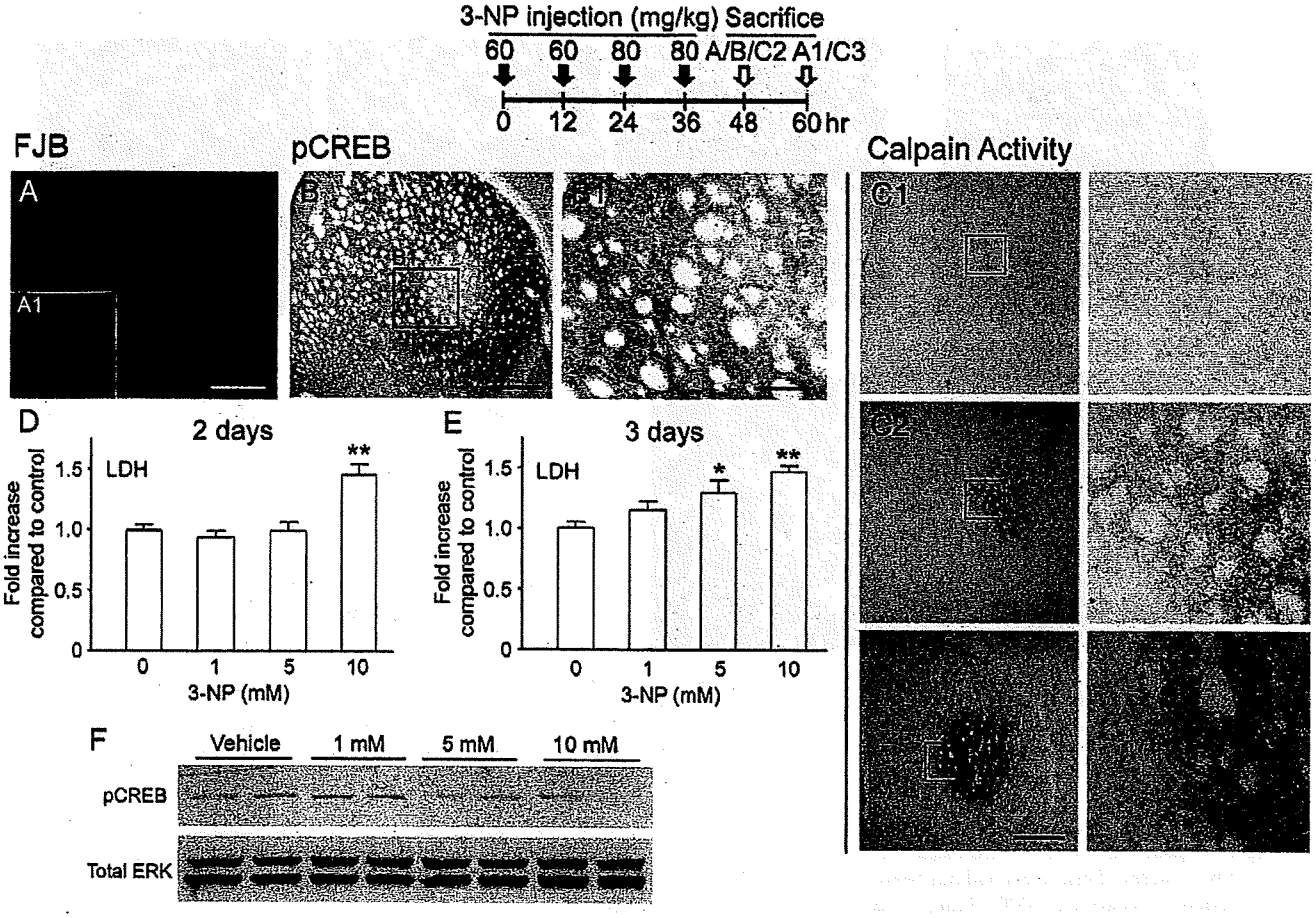

Fig. 3. CREB activity is repressed prior to 3-NP-induced neuronal damage. Top: Time course depicting the 3-NP injection and sacrifice schedule for experiments presented in A, B and C. A. Fluoro-Jade B (FJB) histology did not detect striatal neuronal damage 12 h after the last 3-NP injection. Scale bar: 400 μm. A1 Inset: Representative FJB labeling from a mouse sacrificed 24 h after the last 3-NP injection. Note the marked cell death (denoted by bright green fluorescence) within the dorsolateral striatum. B. pCREB immunolabeling of the adjacent section to the FJB-labeled section in A revealed that CREB activity was elevated within the penumbral region and repressed within the core region. Scale bars: 400 μm in the low magnification image and 100 μm in the enlarged image. C. Representative calpain activity analysis under control conditions (C1) and 12 h (C2) and 24 h (C3) post-NP injection. Boxed regions are shown to the right. Scale bar: 400 μm. D,E. In cultured striatal neurons, LDH release was used to assay 3-NP-evoked cell death. Following 2 days of incubation, 10 mM 3-NP led to a significant increase in cell death relative to the control treatment condition (0 3-NP); after 3 days of incubation, both 5 and 10 mM 3-NP elicited significant cell death relative to the control treatment condition. *, $p<0.05$; **, $p<0.01$. F. After 2 days of incubation with 3-NP, cultured striatal cells were analyzed for pCREB via Western blotting. Administration of 1 mM 3-NP led to a marked increase in pCREB, however, treatment with 5 and 10 mM 3-NP did not increase pCREB levels. To probe for total protein levels, the membrane was stripped and labeled for total erk-1 and erk-2 (total ERK). Data are representative of triplicate determinations.

detected using the Renaissance Chemiluminescent Detection System (New England Nuclear). As a protein loading control, membranes were also probed with a goat polyclonal antibody against total erk-1 and erk-2 (1:2000, Santa Cruz Biotechnology). Membranes were then incubated with an alkaline phosphatase-conjugated secondary antibody and the signal was detected using the Western-CDP Star Chemiluminescent Detection System (Perkin-Elmer).

Results

To induce striatal lesions, mice received a 2-day 3-NP injection paradigm: on the first day, mice were injected twice with 60 mg/kg of 3-NP over a 12 h interval, and with 80 mg/kg at a 12 h interval on the second day (Huang et al., 2006). With this regimen, cresyl violet labeling revealed a distinct lesion 'core' within the lateral striatum 1 day following the final 3-NP injection (Fig. 1A). Maximal cell loss was observed within the mid-striatum (bregma +0.9 to 0.2 mm), with moderate cell loss detected within rostral and caudal regions of the striatum. The pattern of striatal cell loss is consistent with other work examining the effects of 3-NP using the C57/Bl6 line of mice (Fernagut et al., 2002a).

To investigate the role of the CREB/CRE transcriptional pathway in striatal vulnerability to 3-NP, we first examined the expression pattern of the Ser-133 phosphorylated form of CREB (pCREB). Using the 3-NP paradigm described above, and killing mice 1 day after the last injection, we found that pCREB levels were markedly elevated in a 'penumbral' region surrounding the 'core' area of 3-NP-induced cell damage (Fig. 1B). Similar terminology has been used to describe a 3-NP-evoked lesion 'core' where profound cell death occurs, and a 'penumbral' region, where gliosis and limited neuronal survival is observed (Ryu et al., 2003). Double-immunofluorescence labeling for pCREB and NeuN showed that the activated form of CREB was specific to neurons in the penumbral region (Fig. 1C). Expression was significantly elevated relative to the damaged 'core' region as well as more medial striatal regions, which did not exhibit marked signs of cell stress (Fig. 2).

While there is extensive striatal damage 24 h following the last 3-NP injection (Figs. 1A and 3A1), when we examined the striatum at 12 h after the final 3-NP injection, neuronal death measured by Fluoro-Jade B (FJB) staining was not detected (Fig. 3A). Given that FJB is a highly sensitive marker of dead and dying cells (Fig. 3A1), the absence of a FJB signal at the 12 h time point indicates that striatal

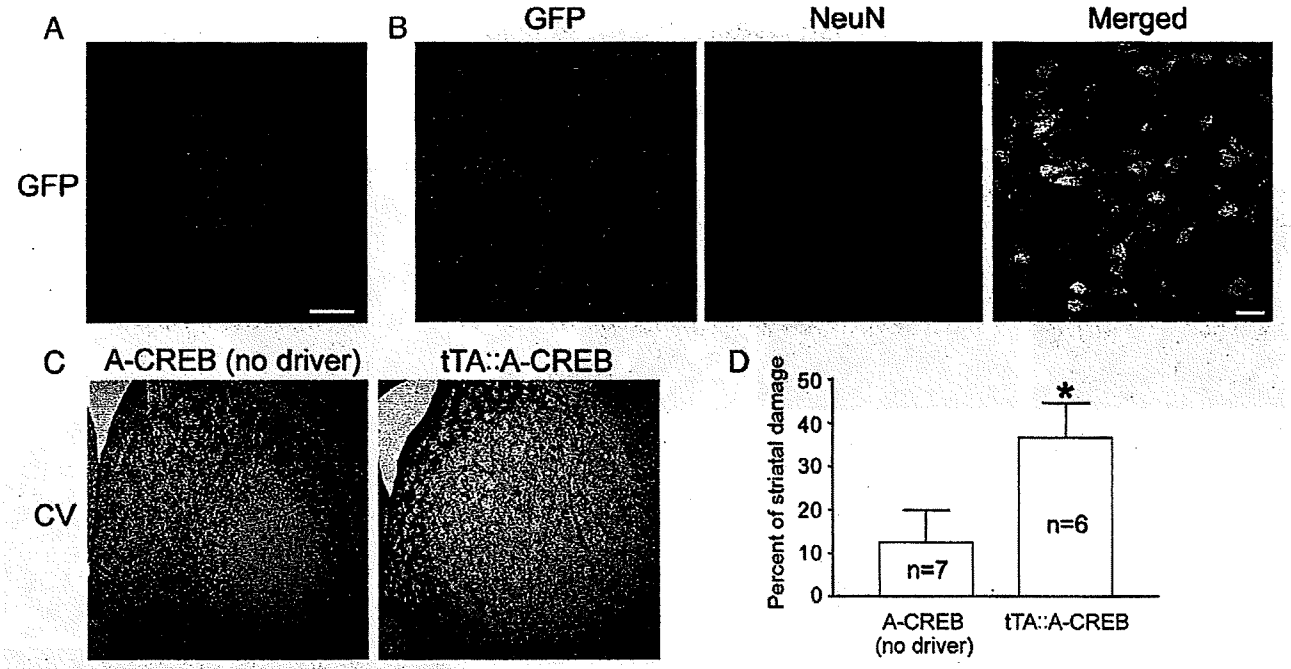

Fig. 4. CREB repression increases 3-NP-evoked cell death. A–B. Striatal expression of the A-CREB/GFP transgenic construct. Low magnification image reveals marked GFP expression within the striatum (A), and double labeling for GFP and NeuN (B) was used to confirm that the transgene is specifically expressed in neurons. Scale bars: 400 μm for A and 20 μm for B. C. Cresyl violet image shows increased striatal damage in tTA::A-CREB mice compared to A-CREB mice lacking the tTA driver. Data were collected 1 day after last 3-NP injection. Scale bar: 400 μm. D. Quantitative analysis of striatal damage in tTA::A-CREB and A-CREB monotransgenic mice. Numbers in the bars refer to the number of animals analyzed. *, $p<0.05$.

tissue was still viable. This analysis was complemented by immunolabeling for calpain enzymatic activity. Calpain activity was of interest because it is a marker of cell stress and has been shown to participate in both apoptotic (Mattson, 2000; Rami, 2003) and nonapoptotic (Mattson 2000; Pang et al., 2003) neuronal death. To this end, tissues collected from both the 12- and 24-h post 3-NP injection time points were immunolabled with an antibody that specifically detects a 136-kDa fragment of α-spectrin (fodrin), which is cleaved by activated calpain (Higuchi et al., 2005). Interestingly, at the 12 h time point modest calpain activity was detected within the core region, whereas at 24 h a marked pattern of calpain activity was detected, and individual immunoreactive cells could be clearly identified (Fig. 3C). These data support the FJB labeling data, indicating that 3-NP evokes a progressive deterioration of striatal cells which culminates in cell death by 24 h following the last 3-NP injection.

Interestingly, at the 12 h post 3-NP injection time point, pCREB expression was repressed in the presumptive core region, relative to the rest of the striatum (Figs. 3B and B1). Furthermore, an increase in pCREB was observed within a penumbra-like region at this time point. This pCREB expression pattern is similar to what is observed at the 24 h time point, indicating that pCREB repression preceded cell death. To directly test the idea that 3-NP can trigger CREB repression prior to neuronal death, we cultured striatal neurons from embryonic day 18 rats and monitored time- and dose-dependent 3-NP-induced cell death using a lactate dehydrogenase (LDH) release assay. Incubation with 10 mM 3-NP for 2 and 3 days triggered significant cell death, while incubation with 5 mM 3-NP triggered significant cell death only following 3 days of incubation; incubation with 1 mM 3-NP did not evoke cell death at either time point (Figs. 3D and F). Using these data as a starting point, we examined pCREB following 2 days of incubation with 3-NP. Interestingly, pCREB was increased by 1 mM 3-NP exposure, but repressed by incubation of 5 or 10 mM 3-NP (Fig. 3F). Since 5 mM 3-NP was not toxic at this 2-day time point, but ultimately led to cell death a day later, these data support the idea that an active mechanism of CREB repression precedes cell death. Thus, these *in vitro* and *in vivo* findings indicate that 3-NP intoxication disrupts CREB phosphorylation, and, in turn, raises the possibility that a subsequent decrease in CREB-mediated transcription contributes to the cell death process.

To test for a potential causative connection between CREB dysregulation and 3-NP-evoked toxicity, we generated a transgenic mouse line (Lee et al., 2007) that expresses a tetracycline-regulated dominant-negative form of CREB (A-CREB; Ahn et al., 1998), as well as the transgene marker protein GFP. Crossing the A-CREB mice with a tetracycline-regulated αCaMKII-tTA activator line (tTA::A-CREB: Mayford et al., 1996) revealed marked transgene expression in the striatum (Fig. 4A). Importantly, only NeuN-positive cells express the transgene (~64%: Lee et al., 2009), indicating that A-CREB expression was neuron-specific (Fig. 4B). Further, we recently reported that transgenic A-CREB represses CRE-mediated transcription and that tonic transgene expression does not alter striatal neuron viability (Lee et al., 2007; 2009). Using cresyl violet staining we observed a much higher degree of 3-NP-evoked tissue damage in tTA::A-CREB mice (~3-fold) compared to A-CREB mice that lacked the driver (tTA) (Figs. 4C and D). Tissue was processed 24 h after the last 3-NP injection. The damage extended in all directions from the lesion locus within the dorsolateral striatum. Next, as an assessment of the effects of A-CREB on neuroprotective gene expression, we analyzed expression of the putative CREB target gene Bcl-2 (Krönke et al., 2003; Wilson et al., 1996) 1 day after the last 3-NP injection. In wild type mice, we noted a marked increase in Bcl-2 expression within the penumbral region (Fig. 5A). Interestingly, in the penumbral region of tTA::A-CREB double-transgenic mice, Bcl-2 expression was largely absent from GFP-positive cells (Fig. 5B), indicating that A-CREB represses Bcl-2 expression.

Next, we assessed motor function in tTA::A-CREB bitransgenic mice and in A-CREB monotransgenic mice. For this study, latency to fall from an accelerating rotarod (2–20 rpm over 300 s) was examined from 1 day before to 4 days after the first 3-NP injection. As shown in Fig. 6A, rotarod performance of 3-NP-treated tTA::

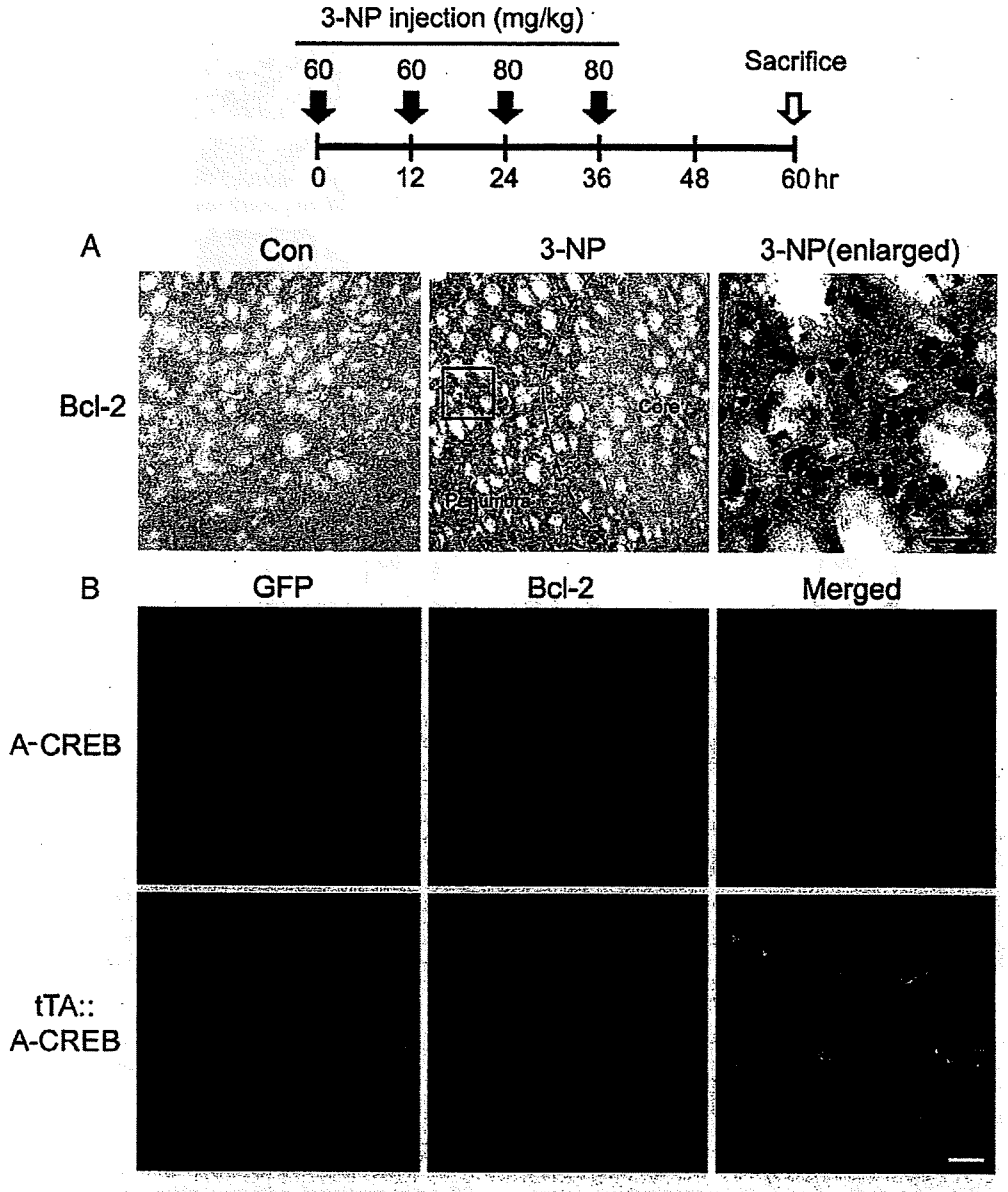

Fig. 5. Neuroprotective gene expression within the penumbral region. Top: time course depicting the 3-NP injection and sacrifice schedule for experiments presented in A and B. A. Relative to vehicle-injected mice, 3-NP intoxication led to a marked increase in Bcl-2 expression within the penumbral region. Dashed line approximates the core/penumbral border. Boxed region is shown to the right. Scale bar: 30 μm. B. Representative double immunofluorescence labeling within the penumbra for Bcl-2 and for the A-CREB transgene marker GFP. Of note, relative to Bcl-2 expression in the monotransgenic A-CREB mouse, modest Bcl-2 expression was observed in the tTA::A-CREB mouse. Further, merging the GFP and Bcl-2 images reveals a lack of overlapping signals, suggesting that A-CREB represses Bcl-2 expression. Scale bar = 20 μm.

A-CREB mice was significantly compromised relative to 3-NP-treated A-CREB mice. Of note, the latency of tTA::A-CREB mice to fall on day 2 of the 3-NP injection was markedly shorter relative to A-CREB monotransgenic mice, and interestingly, over the subsequent 2-day period tTA::A-CREB mice did not show significant recovery in rotarod performance. This contrasts with A-CREB monotransgenic mice, where, on day 4, motor performance had returned to near maximal levels. Together, these data reveal a profound enhancement of 3-NP-induced toxicity and a concordant decrease in motor performance in mice with repressed CREB function.

We next asked whether impaired CREB function affects disease progression in a genetic mouse model of HD. For this study, we used the YAC128 transgenic mouse line (Slow et al., 2003). To generate tri-transgenic mice for YAC128::tTA::A-CREB, we crossed the YAC128 line with tTA::A-CREB double-transgenic mice (representative PCR result are shown in Fig. 6B). Rotarod performance was monitored beginning at 2 months of age in WT nontransgenic littermates, YAC128 transgenic mice and tri-transgenic mice (YAC128::tTA::A-CREB). At 2 months of age there was no significant difference in rotarod performance between control and YAC128 mice (Fig. 6C). However, there was a significant decrease in rotarod performance in tri-transgenic mice compared to control mice at this age. Moving to 6 months of age, the YAC128 mice exhibited an accelerated rate of falling relative to WT littermates. Importantly, the tri-transgenic mice exhibited a significantly enhanced impairment relative to YAC128 mice. These results suggest that CREB function is also critical for the maintenance of motor performance in a genetic model of HD.

The 3-NP data presented above showing that CREB functional repression precedes cell death, and that transgenic disruption of CREB augments cellular toxicity raise the interesting possibility that

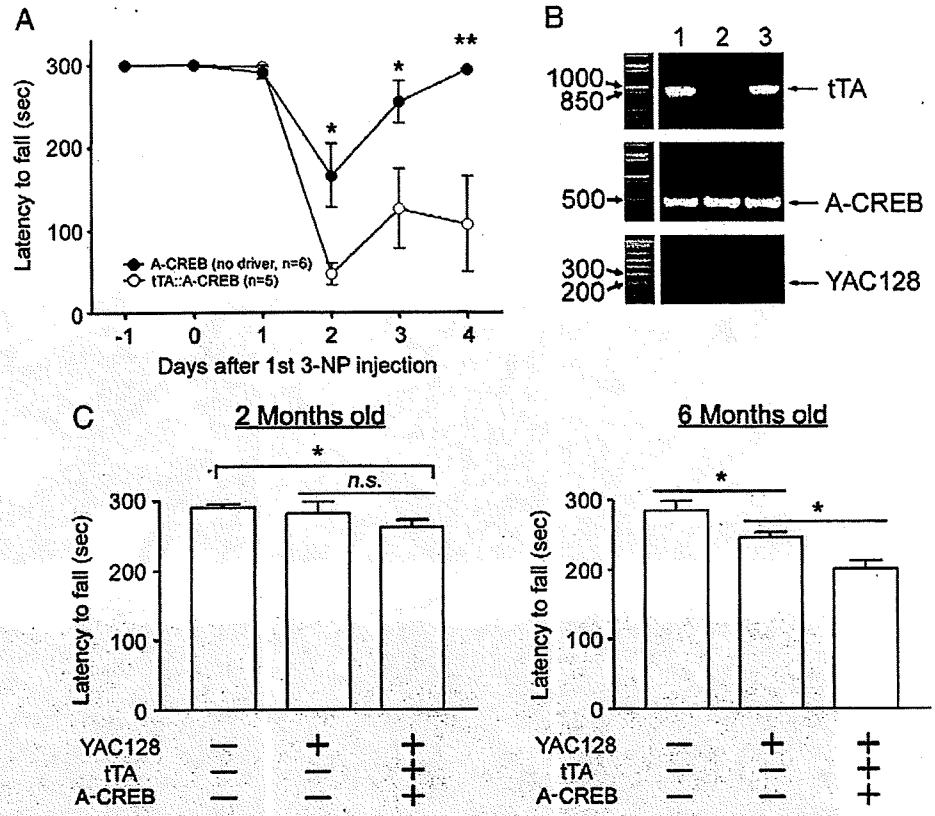

Fig. 6. A-CREB enhances motor deficits. A. Rotarod analysis of 3-NP-evoked fall latency (in seconds) in tTA::A-CREB and A-CREB monotransgenic mice. tTA::A-CREB mice exhibited a significantly decreased fall latency compared to A-CREB monotransgenic mice. *, $p<0.05$; **, $p<0.01$. B. Mouse tail biopsy results for tTA (top), A-CREB/GFP (middle) and YAC128 (bottom) were used to determine the genotypes of three representative mice. Of note, mouse #3 expresses all three transgenes. PCR reactions were run in a 1% agarose gel and visualized using ethidium bromide. C. Rotarod analysis of WT, YAC128 and YAC128:: tTA::A-CREB transgenic mice. (Left) There was no significant difference in fall latency between wild type and YAC128 alone at 2 months of age. However, the YAC128::tTA::A-CREB line showed significantly impaired rotarod performance compared to WT mice. (Right) At 6 months of age, a statistically significant decrease in motor performance was observed in the YAC128 line, relative to WT mice. In addition, the YAC128 phenotype was enhanced by disruption of CREB. Eleven animals were analyzed for the WT line: 11 for the YAC128 line, and 12 for the YAC128:: tTA::A-CREB line. *: $p<0.05$.

therapeutics designed to upregulate CREB function will decrease striatal neurotoxicity. To explore this possibility, we generated mice transgenic for VP16-CREB, a constitutively active form of CREB that binds to the CRE promoter and drives tonic CRE-mediated gene expression (Barco et al., 2002). This construct is analogous to the A-CREB construct, in that it expresses a GFP marker, and, when crossed to the αCaMKII-tTA activator line, drives transgene expression in the striatum (Fig. 7A). With this CREB activator line, we measured the relative extent of 3-NP-induced striatal damage. For this experiment, transgene expression was repressed via the administration of doxycycline (100 μg/mL) from birth to 7 days prior to 3-NP injection. This measure was taken since previous work has shown that chronic expression of VP16-CREB leads to cell death and bouts of epileptiform activity (Lopez et al., 2007). VP16-CREB dramatically attenuated 3-NP-evoked striatal toxicity, as assessed via cresyl violet staining. Thus, at 3 days after the last 3-NP injection, significant cell damage was not detected in 67% of the tTA::VP16-CREB mice ($n=9$), whereas 100% of WT littermates exhibited striatal damage ($n=5$: Figs. 7B and C). To assess motor function, we examined rotarod performance from 1 day before to 3 days after the first 3-NP injection. For these experiments a more aggressive accelerating rotarod training paradigm (4–40 rpm over 300 s) than the one used to test for A-CREB functionality (2–20 rpm) was used, since the motor deficit recovered in a few days after termination of 3-NP injection at the slower acceleration setting (see Fig. 6A). Motor performance in tTA::VP16-CREB mice was significantly better (i.e. longer latency to fall) than WT littermates (Fig. 7D). These data reveal that upregulation of CREB-mediated transcription provides both neuroprotection and improved motor outcome against striatal neurotoxicity.

Discussion

Here we tested the potential role that dysregulation of the CREB/CRE transcriptional pathway plays in the progression of striatal neurodegeneration. To this end, we have focused on the temporal and spatial regulation of CREB activation following cytotoxic striatal stress, and utilized CREB loss- and gain-of-function transgenic mouse models. The findings reported here indicate that 1) a loss of CREB function preceded cell death, 2) abrogation of CREB signaling enhances cytotoxicity, and 3) augmentation of CREB-mediated transcription confers protection against striatal neuronal death.

The rationale for focusing on the CREB/CRE pathway as a route by which to offset HD pathogenesis is grounded in an extensive literature showing that CREB plays a critical role in synapse formation, synaptic transmission, dendritic morphology and neuroprotective gene expression (Huang et al., 2008; Marie et al., 2005; Krönke et al., 2003; Redmond et al., 2002; Shieh et al., 1998; Suzuki et al., 2007;Tao et al., 1998; Wilson et al., 1996). Importantly, these physiological processes and dysregulation of CREB signaling are implicated in HD pathogenesis (DeMarch et al., 2008; Cui et al., 2006; Gines et al., 2003; Jiang et al., 2006; Nucifora et al., 2001; Obrietan and Hoyt 2004; Roze et al., 2008a; Sugars et al., 2004). Further, genetic deletion of CREB triggers an HD-like striatal pathology phenotype (Mantamadiotis et al., 2002), whereas the

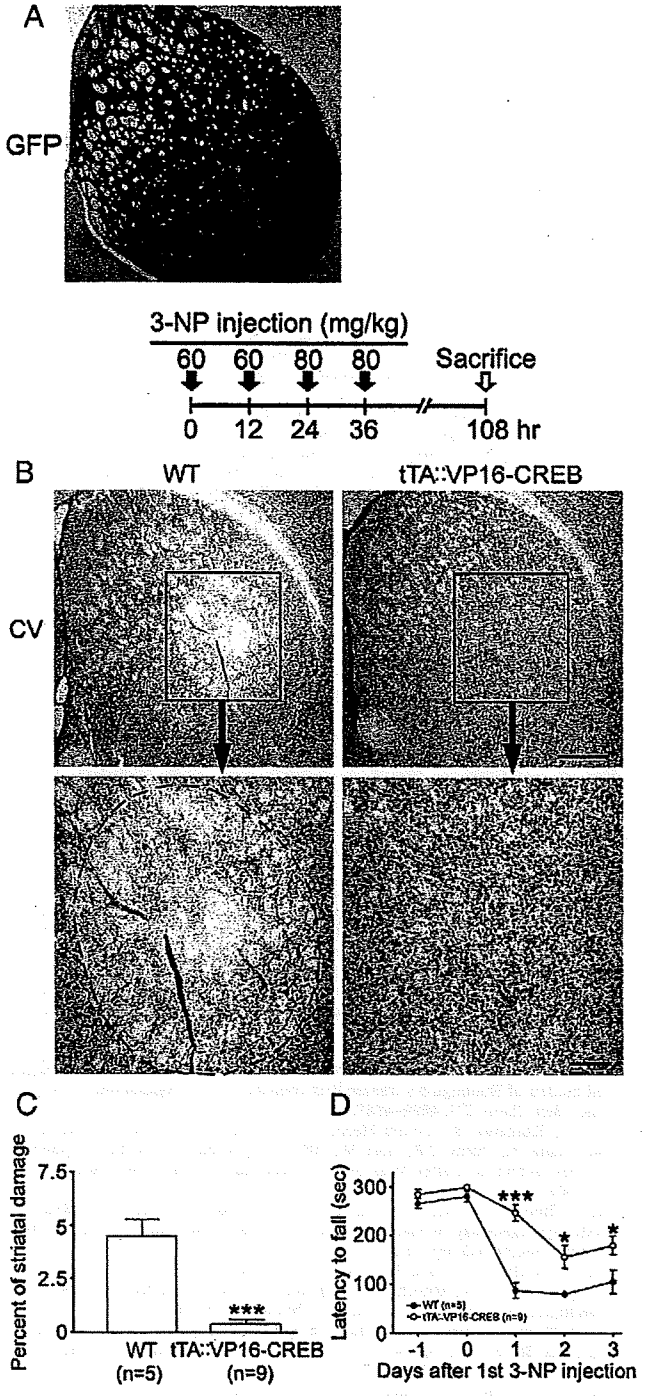

Fig. 7. VP16-CREB confers neuroprotection and improves motor performance. A. Striatal expression of the VP16-CREB/GFP transgenic construct. Immunohistochemical labeling for GFP shows marked transgene expression in the striatum. Scale bar: 400 μm. B. Top: Time course depicting the 3-NP injection and sacrifice schedule. Bottom: Representative cresyl violet images reveal a decrease in the degree of 3-NP-induced striatal damage in tTA::VP16-CREB mice compared to WT mice. Scale bars: 400 μm and 100 μm for the low and high magnification images, respectively. C. Quantitative analysis shows that 3-NP-evoked striatal damage was decreased in tTA::VP16-CREB mice compared to VP16-CREB mice lacking the tTA driver. D. Double-transgenic mice exhibited significantly increased rotarod fall latency compared to WT littermates. *, $p<0.05$; ***, $p<0.001$.

administration of rolipram, which elevates CREB phosphorylation, slows the HD-like pathology in the R6/2 transgenic mouse strain (DeMarch et al., 2008).

Initially, we noted a distinctive pattern of CREB activation in response to 3-NP. pCREB was detected in the penumbral area both before and during active 3-NP-induced striatal neuronal loss, while CREB phosphorylation was repressed in the core region. Core CREB repression appeared to occur prior to cell death, thus suggesting an active mechanism of CREB repression. These findings are consistent with work using ischemia models where the activated form of CREB, as well as CREB-mediated gene transcription, is repressed in the infarct core, but increased in the peri-infarct area (Irving et al., 2000; Sugiura et al., 2004). Likewise, our work showing that Bcl-2 is upregulated in the penumbra, is paralleled by studies showing that ischemia elevates BDNF (a putative CREB-regulated gene) expression outside of the ischemic core (Kokaia et al., 1995). Thus, an active program of CREB-dependent transcription may be a key component of a neuroprotective penumbral 'barrier' that limits the extent of neuronal cell damage. This supposition is supported here by work showing that the repression of CREB signaling dramatically extends the degree of 3-NP-evoked striatal death. Further, apparently conflicting studies (Nucifora et al., 2001; Obrietan and Hoyt, 2004) regarding the regulation of CREB during HD pathogenesis may be resolved by the observations reported here. Hence, mild striatal pathology (i.e., within the 3-NP-induced penumbra) triggers neuroprotective CREB-dependent transcription, whereas more progressive striatal degeneration (i.e., within the 3-NP-induced core) leads to an active program of CREB repression, which, in turn facilitates neuronal pathogenesis.

As a complement to the 3-NP studies, we report impaired rotarod performance as early as 2 months of age in tri-transgenic mice (YAC128::tTA::A-CREB), compared to WT mice and at 6 months the tri-transgenic mice were significantly more impaired than YAC128 mice. These data are highly suggestive of an important role of CRE-dependent transcription in protection against the toxic effects of mutant huntingtin *in vivo*. Further, given the potent neuroprotective effect of VP16-CREB on 3-NP-induced striatal lesions, it is reasonable to postulate that transgenic upregulation of CREB-mediated gene expression would also confer a marked neuroprotective effect against mutant huntingtin. Future studies will examine gene expression patterns and striatal pathology in YAC128 mice that have either activated or repressed CREB.

In conclusion, the observation that upregulation of CREB-dependent transcription reduces striatal cell death and facilitates behavioral recovery provides a strong rationale for the development of therapeutic approaches designed to affect CREB-dependent transcription.

Acknowledgments

This work was supported by the National Institutes of Health (Grant numbers: NS47176 and 5P30NS045758) and a Post-Doctoral Fellowship for Y-S. C. from the Hereditary Disease Foundation.

References

Ahn, S., Olive, M., Aggarwal, S., Krylov, D., Ginty, D.D., Vinson, C., 1998. A dominant-negative inhibitor of CREB reveals that it is a general mediator of stimulus-dependent transcription of c-*fos*. Mol. Cell. Biol. 18, 967–977.

Barco, A., Alarcon, J.M., Kandel, E.R., 2002. Expression of constitutively active CREB protein facilitates the late phase of long-term potentiation by enhancing synaptic capture. Cell 108, 689–703.

Beal, M.F., Brouillet, E., Jenkins, B.G., Ferrante, R.J., Kowall, N.W., Miller, J.M., Storey, E., Srivastava, R., Rosen, B.R., Hyman, B.T., 1993. Neurochemical and histologic characterization of striatal excitotoxic lesions produced by the mitochondrial toxin 3-nitropropionic acid. J. Neurosci. 13, 4181–4192.

Cha, J.H., 2007. Transcriptional signatures in Huntington's disease. Prog. Neurobiol. 83, 228–248 Review..

Choi, Y.S., Lin, S.L., Lee, B., Kurup, P., Cho, H.Y., Naegele, J.R., Lombroso, P.J., Obrietan, K., 2007. Status epilepticus-induced somatostatinergic hilar interneuron degeneration is regulated by striatal enriched protein tyrosine phosphatase. J. Neurosci. 27, 2999–3009.

Cui, L., Jeong, H., Borovecki, F., Parkhurst, C.N., Tanese, N., Krainc, D., 2006.

Transcriptional repression of PGC-1alpha by mutant huntingtin leads to mitochondrial dysfunction and neurodegeneration. Cell 127, 59–69.
DeMarch, Z., Giampà, C., Patassini, S., Martorana, A., Bernardi, G., Fusco, F.R., 2007. Beneficial effects of rolipram in a quinolinic acid model of striatal excitotoxicity. Neurobiol. Dis. 25, 266–273.
DeMarch, Z., Giampà, C., Patassini, S., Bernardi, G., Fusco, F.R., 2008. Beneficial effects of rolipram in the R6/2 mouse model of Huntington's disease. Neurobiol. Dis. 30, 375–387.
Fernagut, P.O., Diguet, E., Stefanova, N., Biran, M., Wenning, G.K., Canioni, P., Bioulac, B., Tison, F., 2002a. Subacute systemic 3-nitropropionic acid intoxication induces a distinct motor disorder in adult C57Bl/6 mice: behavioural and histopathological characterisation. Neurosci. 114, 1005–1017.
Fernagut, P.O., Diguet, E., Jaber, M., Bioulac, B., Tison, F., 2002b. Dopamine transporter knock-out mice are hypersensitive to 3-nitropropionic acid-induced striatal damage. Eur. J. Neurosci. 15, 2053–2056.
Gil, J.M., Rego, A.C., 2008. Mechanisms of neurodegeneration in Huntington's disease. Eur. J. Neurosci. 27, 2803–2820.
Gines, S., Seong, I.S., Fossale, E., Ivanova, E., Trettel, F., Gusella, J.F., Wheeler, V.C., Persichetti, F., MacDonald, M.E., 2003. Specific progressive cAMP reduction implicates energy deficit in presymptomatic Huntington's disease knock-in mice. Hum. Mol. Genet. 12, 497–508.
Higgins, D.S., Hoyt, K.R., Baic, C., Vensel, J., Sulka, M., 1999. Metabolic and glutamatergic disturbances in the Huntington's disease transgenic mouse. Ann. N.Y. Acad. Sci. 893, 298–300.
Higuchi, M., Tomioka, M., Takano, J., Shirotani, K., Iwata, N., Masumoto, H., Maki, M., Itohara, S., Saido, T.C., 2005. Distinct mechanistic roles of calpain and caspase activation in neurodegeneration as revealed in mice overexpressing their specific inhibitors. J. Biol. Chem. 280, 15229–15237.
Huang, Q.Y., Wei, C., Yu, L., Coelho, J.E., Shen, H.Y., Kalda, A., Linden, J., Chen, J.F., 2006. Adenosine A2A receptors in bone marrow-derived cells but not in forebrain neurons are important contributors to 3-nitropropionic acid-induced striatal damage as revealed by cell-type-selective inactivation. J. Neurosci. 26, 11371–11378.
Huang, Y.H., Lin, Y., Brown, T.E., Han, M.H., Saal, D.B., Neve, R.L., Zukin, R.S., Sorg, B.A., Nestler, E.J., Malenka, R.C., Dong, Y., 2008. CREB modulates the functional output of nucleus accumbens neurons: a critical role of N-methyl-D-aspartate glutamate receptor (NMDAR) receptors. J. Biol. Chem. 283, 2751–2760.
Irving, E.A., Barone, F.C., Reith, A.D., Hadingham, S.J., Parsons, A.A., 2000. Differential activation of MAPK/ERK and p38/SAPK in neurones and glia following focal cerebral ischaemia in the rat. Brain Res. Mol. Brain Res. 77, 65–75.
Jiang, H., Poirier, M.A., Liang, Y., Pei, Z., Weiskittel, C.E., Smith, W.W., DeFranco, D.B., Ross, C.A., 2006. Depletion of CBP is directly linked with cellular toxicity caused by mutant huntingtin. Neurobiol. Dis. 23, 543–551.
Koh, J.Y., Choi, D.W., 1987. Quantitative determination of glutamate mediated cortical neuronal injury in cell culture by lactate dehydrogenase efflux assay. J. Neurosci. Methods 20, 83–90.
Kokaia, Z., Zhao, Q., Kokaia, M., Elmér, E., Metsis, M., Smith, M.L., Siesjö, B.K., Lindvall, O., 1995. Regulation of brain-derived neurotrophic factor gene expression after transient middle cerebral artery occlusion with and without brain damage. Exp. Neurol. 136, 73–88.
Krönke, G., Bochkov, V.N., Huber, J., Gruber, F., Blüml, S., Fürnkranz, A., Kadl, A., Binder, B.R., Leitinger, N., 2003. Oxidized phospholipids induce expression of human heme oxygenase-1 involving activation of cAMP-responsive element-binding protein. J. Biol. Chem. 278, 51006–51014.
Lee, B., Butcher, G.Q., Hoyt, K.R., Impey, S., Obrietan, K., 2005a. Activity-dependent neuroprotection and cAMP response element-binding protein (CREB): kinase coupling, stimulus intensity, and temporal regulation of CREB phosphorylation at serine 133. J. Neurosci. 25, 1137–1148.
Lee, J., Kim, C.H., Simon, D.K., Aminova, L.R., Andreyev, A.Y., Kushnareva, Y.E., Murphy, A.N., Lonze, B.E., Kim, K.S., Ginty, D.D., Ferrante, R.J., Ryu, H., Ratan, R.R., 2005b. Mitochondrial cyclic AMP response element-binding protein (CREB) mediates mitochondrial gene expression and neuronal survival. J. Biol. Chem. 280, 40398–40401.
Lee, B., Dziema, H., Lee, K.H., Choi, Y.S., Obrietan, K., 2007. CRE-mediated transcription and COX-2 expression in the pilocarpine model of status epilepticus. Neurobiol. Dis. 25, 80–91.
Lee, B., Cao, R., Choi, Y.S., Cho, H.Y., Rhee, A.D., Hah, C.K., Hoyt, K.R., Obrietan, K., 2009. The CREB/CRE transcriptional pathway: protection against oxidative stress-mediated neuronal cell death. J. Neurochem. 108, 1251–1265.
Lopez de Armentia, M., Jancic, D., Olivares, R., Alarcon, J.M., Kandel, E.R., Barco, A., 2007. cAMP response element-binding protein-mediated gene expression increases the intrinsic excitability of CA1 pyramidal neurons. J. Neurosci. 27, 13909–13918.
Mantamadiotis, T., Lemberger, T., Bleckmann, S.C., Kern, H., Kretz, O., Martin Villalba, A., Tronche, F., Kellendonk, C., Gau, D., Kapfhammer, J., Otto, C., Schmid, W., Schütz, G., 2002. Disruption of CREB function in brain leads to neurodegeneration. Nat. Genet. 31, 47–54.
Marie, H., Morishita, W., Yu, X., Calakos, N., Malenka, R.C., 2005. Generation of silent synapses by acute in vivo expression of CaMKIV and CREB. Neuron 45, 741–752.
Mattson, M.P., 2000. Apoptosis in neurodegenerative disorders. Nat. Rev. Mol. Cell Biol. 1, 120–129.
Mayford, M., Bach, M.E., Huang, Y.Y., Wang, L., Hawkins, R.D., Kandel, E.R., 1996. Control of memory formation through regulated expression of a CaMKII transgene. Science 274, 1678–1683.
Nucifora Jr., F.C., Sasaki, M., Peters, M.F., Huang, H., Cooper, J.K., Yamada, M., Takahashi, H., Tsuji, S., Troncoso, J., Dawson, V.L., Dawson, T.M., Ross, C.A., 2001. Interference by huntingtin and atrophin-1 with CBP-mediated transcription leading to cellular toxicity. Science 291, 2423–2428.
Obrietan, K., Hoyt, K.R., 2004. CRE-mediated transcription is increased in Huntington's disease transgenic mice. J. Neurosci. 24, 791–796.
Pang, Z., Bondada, V., Sengoku, T., Siman, R., Geddes, J.W., 2003. Calpain facilitates the neuron death induced by 3-nitropropionic acid and contributes to the necrotic morphology. J Neuropathol. Exp. Neurol. 62, 633–643.
Rami, A., 2003. Ischemic neuronal death in the rat hippocampus: the calpain–calpastatin–caspase hypothesis. Neurobiol. Dis. 13, 75–88.
Redmond, L., Kashani, A., Ghosh, A., 2002. Calcium regulation of dendritic growth via Cam kinase IV and CREB-mediated transcription. Neuron 34, 999–1010.
Roze, E., Betuing, S., Deyts, C., Marcon, E., Brami-Cherrier, K., Pagès, C., Humbert, S., Mérienne, K., Caboche, J., 2008a. Mitogen- and stress-activated protein kinase-1 deficiency is involved in expanded-huntingtin-induced transcriptional dysregulation and striatal death. FASEB J. 22, 1083–1093.
Roze, E., Saudou, F., Caboche, J., 2008b. Pathophysiology of Huntington's disease: from huntingtin functions to potential treatments. Curr. Opin. Neurol. 21, 497–503 Review..
Ryu, J.K., Nagai, A., Kim, J., Lee, M.C., McLarnon, J.G., Kim, S.U., 2003. Microglial activation and cell death induced by the mitochondrial toxin 3-nitropropionic acid: in vitro and in vivo studies. Neurobiol. Dis. 12, 121–132.
Saulle, E., Gubellini, P., Picconi, B., Centonze, D., Tropepi, D., Pisani, A., Morari, M., Marti, M., Rossi, L., Papa, M., Bernardi, G., Calabresi, P., 2004. Neuronal vulnerability following inhibition of mitochondrial complex II: a possible ionic mechanism for Huntington's disease. Mol. Cell. Neurosci. 25, 9–20.
Semaka, A., Creighton, S., Warby, S., Hayden, M.R., 2006. Predictive testing for Huntington disease: interpretation and significance of intermediate alleles. Clin. Genet. 70, 283–294 Review.
Shieh, P.B., Hu, S.C., Bobb, K., Timmusk, T., Ghosh, A., 1998. Identification of a signaling pathway involved in calcium regulation of BDNF expression. Neuron 20, 727–740.
Slow, E.J., van Raamsdonk, J., Rogers, D., Coleman, S.H., Graham, R.K., Deng, Y., Oh, R., Bissada, N., Hossain, S.M., Yang, Y.Z., Li, X.J., Simpson, E.M., Gutekunst, C.A., Leavitt, B.R., Hayden, M.R., 2003. Selective striatal neuronal loss in a YAC128 mouse model of Huntington disease. Hum. Mol. Genet. 12, 1555–1567.
St Pierre, J, Drori, S, Uldry, M, Silvaggi, JM, Rhee, J, Jäger, S, Handschin, C, Zheng, K, Lin, J, Yang, W, Simon, DK, Bachoo, R, Spiegelman, BM, 2006. Suppression of reactive oxygen species and neurodegeneration by the PGC-1 transcriptional coactivators. Cell 127, 397–408.
Sugars, K.L., Brown, R., Cook, L.J., Swartz, J., Rubinsztein, D.C., 2004. Decreased cAMP response element-mediated transcription: an early event in exon 1 and full-length cell models of Huntington's disease that contributes to polyglutamine pathogenesis. J. Biol. Chem. 279, 4899–4988.
Sugiura, S., Kitagawa, K., Omura-Matsuoka, E., Sasaki, T., Tanaka, S., Yagita, Y., Matsushita, K., Storm, D.R., Hori, M., 2004. CRE-mediated gene transcription in the peri-infarct area after focal cerebral ischemia in mice. J. Neurosci. Res. 75, 401–407.
Suzuki, S., Zhou, H., Neumaier, J.F., Pham, T.A., 2007. Opposing functions of CREB and MKK1 synergistically regulate the geometry of dendritic spines in visual cortex. J. Comp. Neurol. 503, 605–617.
Tabrizi, S.J., Workman, J., Hart, P.E., Mangiarini, L., Mahal, A., Bates, G., Cooper, J.M., Schapira, A.H., 2000. Mitochondrial dysfunction and free radical damage in the Huntington R6/2 transgenic mouse. Ann. Neurol. 47, 80–86.
Tao, X., Finkbeiner, S., Arnold, D.B., Shaywitz, A.J., Greenberg, M.E., 1998. Ca2+ influx regulates BDNF transcription by a CREB family transcription factor-dependent mechanism. Neuron 20, 709–726.
Wilson, B.E., Mochon, E., Boxer, L.M., 1996. Induction of bcl-2 expression by phosphorylated CREB proteins during B-cell activation and rescue from apoptosis. Mol. Cell. Biol. 16, 5546–5556.